ErbB2/HER2 governs CDK4 inhibitor sensitivity and timing and irreversibility of G1/S transition by altering c-Myc and cyclin D function

Authors: Ayaka Nagasato-Ichikawa[1], Ken Murakami[1], Kazuhiro Aoki[2,3], Mariko Okada[1]*

Affiliations:

[1]Laboratory for Cell Systems, Institute for Protein Research, Osaka University, Suita, Osaka 565-0871, Japan

[2]Exploratory Research Center on Life and Living Systems (ExCELLS), National Institutes of Natural Sciences, Okazaki, Japan; National Institute for Basic Biology, National Institutes of Natural Sciences, Okazaki, Japan; Department of Basic Biology, School of Life Science, SOKENDAI (The Graduate University for Advanced Studies), Okazaki 444-8787, Japan

[3]Graduate School of Biostudies, Kyoto University, Kyoto 606-8501, Japan

*Corresponding author: mokada@protein.osaka-u.ac.jp

Abstract:

Cell cycle entry and irreversible transition from the G1 to S phase are crucial for mammalian cell proliferation. The ErbB receptor (ErbB1/2/3/4) pathway plays an important role in the proliferation of human cancer cells, and increased ErbB2/HER2 activity is often observed in malignant breast cancer. However, the mechanisms underlying the ErbB2-mediated G1/S transition remain incompletely characterized, as this process is tightly modulated by crosstalk between pathways, transcription factors, and feedback loops. Here, we performed an extensive time-course analysis of high and low ErbB2-expressing breast cancer cells to reveal the regulation of the growth factor-induced G1/S transition. Live-cell imaging using cell cycle reporters revealed that the G1/S transition occurs 20 h after ErbB2 activation, driven primarily by the cyclin D1/CDK4-RB axis. Additionally, ErbB2 protein stability was found to be maintained by Hsp90, which is modulated by CDK4 at this time point. CDK4 inhibitor treatment induced cell cycle arrest in most cells, but a subpopulation exhibited the G1/S transition with a 25 h-delay caused by c-Myc activation through epigenetic modifications. Conversely, in the cells with high ErbB2 expression, CDK4 inhibition led to an excessive increase in c-Myc transcriptional activity, a rapid decrease in cyclin D1 expression, and abolishment of cell cycle arrest. Overall, our study offers a comprehensive account of how ErbB2 receptor levels modulate the roles of cyclin D1 and c-Myc in the G1/S transition. These results suggest that variations in ErbB2 levels within breast cancer tissues reflect heterogeneity in sensitivity to CDK4 inhibitors, potentially complicating treatment strategies.

One Sentence Summary: CDK4 inhibition paradoxically activates c-Myc and reverses cell cycle arrest in high ErbB2-expressing breast cancer cells.

Main Text:

INTRODUCTION

The initiation of the cell cycle and the subsequent transition from the G1 to S phase are regulated by an interwoven molecular network involving the formation of a cyclin D1/CDK4 protein complex (*1–3*). Understanding the regulation of the G1/S transition by mitogenic signals is fundamental in the field of cell biology and essential for developing cancer treatments and overcoming drug resistance. Cyclin D1 overexpression has been known to enhance breast cancer cell proliferation (*4*). Consequently, cell cycle inhibitors targeting CDK4 have been developed to treat breast cancer patients (*5*, *6*).

Breast cancer can be classified into four subtypes based on the expression of estrogen receptors (ERs), progesterone receptors (PRs), and ErbB2 (HER2) receptors: luminal A (ER^+ and $HER2^-$), luminal B (ER^+ and $HER2^+$), ErbB2/HER2 positive (ER^- and $HER2^+$), and triple-negative (ER^- and $HER2^-$) (*7–9*). Among these, CDK4 inhibitors (CDK4is) have been used to treat the luminal A subtype (*5*, *10*). However, long-term administration of CDK4is has led to drug resistance, mainly due to activation of signaling pathways, such as PI3K/AKT/mTOR and Hippo, and non-coding RNA regulation (*11–21*). Increased activity of the ErbB2 tyrosine kinase is also commonly observed in malignant breast cancer, and ErbB2 is known to elevate cyclin D1 levels (*22*, *23*). A major subset of ErbB2-overexpressing cells is found within the luminal A subtype, typically characterized by low ErbB2 levels (*24*). Therefore, we speculated that a small population of high ErbB2-expressing cells in the luminal A subtype may contribute to CDK4i resistance by rewiring the G1/S network to escape cell cycle arrest. However, it remains unclear which molecules in the G1/S network are affected by the ErbB2 receptor and how these alterations influence the decision at the G1/S transition, particularly regarding cell cycle entry or arrest.

Stimulation of ErbB2 receptors activates the MAPK/ERK and PI3K/AKT signaling pathways, leading to the rapid induction of early-response genes such as c-Fos and c-Myc (*25–27*). These transcription factors play a key role in regulating the expression of cyclin D1 and CDK4 (*27–29*). Both c-Myc and cyclin D1 are involved in the regulation of the G1/S transition. However, they appear to have distinct roles in this process (*30*). The G1/S transition typically involves the signal-dependent and -independent processes. Moreover, between these processes is a boundary known as the restriction point (R point) (*2*, *31*).

The mitogenic signal primarily regulates the expression and activation of cyclin D1/CDK4, which phosphorylates retinoblastoma protein (RB) prior to the R point. Thus, this signal-dependent process is primarily driven by the cyclin D1/CDK4-RB axis (*2*). The phosphorylation (p-RB) activates E2F1, promoting expression of its target genes, including cyclin E. Cyclin E then forms a complex with CDK2, which further phosphorylates p-RB, resulting in a fully phosphorylated state (pp-RB). This complete phosphorylation amplifies E2F1 activity. The

resulting positive feedback loop involving cyclin E/CDK2, RB, and E2F1 is thought to function independently of mitogenic signaling (*32*, *33*). However, the expression and stability of c-Myc are modulated by external signals (*34*), and c-Myc directly influences E2F1 promoter activity (*35*). Consequently, the core machinery of the cyclin E/CDK2-RB-E2F1 is also considered to be indirectly regulated by mitogenic signals. Furthermore, cyclin D1/CDK4 is necessary to sustain RB inactivation beyond the R point, indicating a broader influence of the signal on cell cycle progression from the G1 to the G2 phase (*36*).

The expression of c-Myc and cyclin D1 is controlled by ERK (*37*, *38*), and their protein stability is regulated by AKT activity (*37*, *39*). On the other hand, p27, which plays a crucial role in the accumulation of cyclin D1 and CDK4 during the G1 phase (*40*), is known to be repressed by c-Myc (*41*). As the ErbB2 receptor activates ERK and AKT pathways at different magnitudes (*42*), different levels of ErbB2 may influence the abundance of the cyclin D1 and c-Myc, thereby affecting their dependence at the G1/S transition. In other words, the ErbB2 receptor possibly modulates the core machinery of the G1/S network and influences the timing and decision of cell cycle entry through modulation of cyclin D1 and c-Myc. Therefore, examining the ratio of c-Myc to cyclin D1 at the single-cell level may shed light on their roles in the G1/S transition, the mechanism of drug resistance to CDK4is, and the role of ErbB2 in this process.

In the present study, we used representative luminal A subtype cell lines (MCF-7 and T47D), which express low levels of the ErbB1 receptor (EGFR) and high levels of the ErbB3 receptor (*27*, *42*, *43*). ErbB2 is an orphan receptor activated by heterodimerization with ErbB3, ErbB4, or EGFR (*26*). Stimulation with the ErbB3 ligand, heregulin (HRG), triggers the heterodimerization of ErbB2 and ErbB3, thereby activating the ERK and AKT pathways (*42*). We conducted an extensive time-course analysis of proteins and their phosphorylation status regarding cell cycle regulators and transcription factors following HRG stimulation, examining the S phase entry, together with live-cell imaging using fluorescent ubiquitination-based cell cycle indicator (FUCCI) to quantitatively analyze the cell cycle dynamics in the presence of CDK4i. Additionally, we performed transcriptome and epigenetic analyses to identify the transcription factor determining cell cycle entry under drug inhibition conditions. Ultimately, we assessed the effect of ErbB2 levels on the regulation of timing and irreversibility of the G1/S transition.

RESULTS

G1/S transition occurs approximately 20 h after HRG stimulation

First, we investigated the timing of cell cycle transition after HRG stimulation. To analyze the cell cycle dynamics, we established a live-cell imaging analysis system in which the FUCCI (*44*) was stably expressed in MCF-7 to observe real-time changes in the cell cycle (Fig. 1A). Next, we analyzed the distribution of each cell cycle phase in the presence or absence of HRG for up to 72 h (Fig. 1B to D). Compared to that in the control, the proportion of cells in the S/G2/M phase began to increase significantly after 24 h of HRG stimulation. Additionally, the number of nuclei, serving as a readout of cell number, increased 1.4-fold after 48 h, suggesting that HRG stimulation enhances cell proliferation. Conversely, control cells showed a gradual increase in the proportion of S/G2/M cells over time, but there was no increase in the number of nuclei, suggesting cell cycle arrest in the S/G2/M phase in the absence of the ligand. To further examine the transition times of each phase of the cell cycle following HRG stimulation, we performed single-cell tracking and quantified the distribution of the cell cycle phases (Fig. 1E; Fig. S1A and B). Our results indicated that the G1/S transition occurred at 19.0 ± 7.2 h after HRG stimulation. In comparison, the S/G2 and M/G1 transitions occurred at 32.5 ± 9.3 h and 39.4 ± 8.7 h, respectively (Fig. 1F). These findings suggested that most cells entered the S phase approximately 20 h after HRG stimulation, with a degree of intercellular variability.

CDK4 and cyclin D1 proteins are expressed in a timely manner at the G1/S transition

We further examined the signaling dynamics of ErbB2, AKT, and ERK pathways (*26*, *45*) following HRG stimulation (Fig. 2A and B; Fig. S2A). The results showed that phospho-ErbB2 (p-ErbB2) levels peaked within 30 min of HRG stimulation, rapidly decreased within 2 h, and gradually increased until the S/G2/M transition point (32 h). Similarly, the levels of p-AKT and p-ERK peaked within 30 min, followed by a gradual decrease in p-AKT levels over approximately 12 h and a rapid reduction in p-ERK levels within 4 h. Both kinases maintained moderate phosphorylation levels until the attainment of the S/G2/M transition point. The levels of c-Myc and p-c-Myc (Ser^{62}) peaked within 2 h of HRG stimulation and then decreased to baseline levels until the G1/S transition point was reached (20 h). Conversely, although c-Fos protein expression levels peaked within 2 h and quickly reduced to basal levels, p-c-Fos showed dynamics similar to those of p-ERK, maintaining a moderate phosphorylation level until the S/G2/M transition. Following ErbB2 activation, p-AKT, p-ERK, and p-c-Fos levels were maintained for a prolonged period until the S/G2/M transition, whereas c-Myc and p-c-Myc levels decreased around the time of the G1/S transition.

Next, we estimated the timing of the R point from the expression and phosphorylation dynamics of cell cycle regulator proteins (Fig. 2C and D; Fig. S2B). Cyclin D1/CDK4 activity is required to maintain RB inactivation from the G1 to G2 phase. Here, the protein levels of cyclin D1 and CDK4 began to increase shortly after HRG stimulation; they peaked approximately 20 h after

HRG stimulation and then gradually decreased (Fig. 2D). p-RB (Thr^{373}) (*46*) showed a time-course pattern similar to that of cyclin D1/CDK4, whereas p-RB ($Ser^{807/811}$) showed a monotonic increase similar to that of cyclin E (Fig. S2C and D), suggesting different roles for each phosphorylation site in the regulation of G1/S transition and cyclin E expression. Conversely, E2F1 expression increased similar to that of cyclin E and CDK2 (Fig. S2C and D) in the time frame of 12–20 h after HRG stimulation. Thus, our results confirmed that cyclin D1/CDK4 may play a role in maintaining RB phosphorylation near the R point, which is critical for the initial step in progressing toward the G1/S transition associated with HRG-induced ErbB2 activation.

A subset of the population enters the cell cycle even after CDK4 inhibition

Next, we investigated whether cyclin D1/CDK4 is necessary for the HRG-stimulated G1/S transition in the MCF-7 cells. As the R point may exist approximately 12 to 16 h after HRG stimulation, cells were treated with a CDK4i (250 nM, a concentration that inhibited approximately 50% of the HRG-induced cyclin D1 expression) 12 h after HRG stimulation (Fig. S3A and B). As ERK activates cyclin D1 expression and AKT inhibits its degradation (*47*), we used 600 nM AKT inhibitor (AKTi) and 500 nM MEK inhibitor (MEKi), which have comparable inhibitory effects on cyclin D1 expression (Fig. S3A and B), as CDK4i. We examined the proportion of cells in each cell cycle phase at the early (32 h) and late (72 h) time points after HRG stimulation (Fig. 3A and B). At early time points, fewer cells treated with CDK4i (13.8%), AKTi (7.05%), or MEKi (13.8%) were in the S/G2/M phase compared to non-treated cells (29.2%). However, at later time points, although AKTi (9.85%) and MEKi (5.50%) reduced the proportion of cells in the S/G2/M phase, CDK4i (17.7%) did not show a similar effect. Furthermore, after 72 h, the number of nuclei was significantly reduced by AKTi and MEKi but not by CDK4i (Fig. 3C). This indicates that AKTi and MEKi can induce growth inhibition or cell death in most cell populations. While CDK4i induced cell cycle arrest in most cells, a small subset of cells (17.7%) did not respond and continued to progress, suggesting that additional mechanisms maintain the cell cycle functionality in the absence of CDK4.

If a distinct mechanism were responsible for progress of the G1/S entry during CDK4 inhibitor treatment, the correlation between the G1/S and other phase transitions would likely differ from that observed during AKT or MEK inhibitor treatments. To evaluate this hypothesis, we tested a correlation between the timing of G1/S and M/G1 transition for each inhibitor treatment for up to 72 h (Fig. 3D). The average time to G1/S transition was longer in the CDK4i treatment (49.5 ± 13.2) than in control (24.7 ± 5.7), AKTi (39.6 ± 14.8), and MEKi (26.6 ± 11.5) conditions (Fig. 3D). Thus, non-responders to CDK4i significantly delayed the time to G1/S transition by approximately 25 h in comparison to the control. Pearson's correlation coefficients between the time to G1/S and the time to M/G1 were significantly lower for CDK4i (0.76) than for AKTi (0.91), MEKi (0.95), and control conditions (0.84). Furthermore, the slope (s) of the regression equation reflects the relationship between the G1/S transition time and the M/G1 transition time,

while the intercept (i) reflects the length of time it takes to reach the M/G1 transition point. As a result, the slope (s) and intercept (i) of the regression equation also exhibited a lower slope (s = 0.56) and higher intercept (i = 37) in the CDK4i condition than in the AKTi (s = 1.0, i = 19), MEKi (s = 0.95, i = 17), and control conditions (s = 1.0, i = 17). The result implies that the duration of the G1/S to G2/M phase may not be uniformly controlled only by CDK4i, and there might be a phase-specific regulation.

The CDK4i condition showed a clear negative correlation between the time to G1/S transition and the duration of the S/G2/M phase (Fig. 3E). We divided the cell population into the early and late groups based on the median time of each G1/S transition (CDK4i; 49.5 ± 13.2, AKTi; 39.6 ± 14.8, MEKi; 26.6 ± 11.5, Control; 24.7 ± 5.7) and compared with the duration of each S, G2, and M phase (Fig. S3C). The mean duration of S/G2/M differed significantly between the early (22.3 ± 7.2) and the late (15.8 ± 2.4) groups with a 6 h-difference observed only CDK4i treatment and not with other inhibitors. Thus, in this CDK4i-specific response, the majority of CDK4i non-responders showed a long G1/S and a short S/G2/M phase. We also observed that another luminal A T47D cells (which express a moderate level of ErbB2) required 32.6 ± 12.2 h to reach the G1/S transition under CDK4i treatment, compared to 21.62 ± 6.2 in the control condition (Fig. S3D to F).

CDK4i enhances c-Myc transcriptional activity via H3K27Ac modification

The regulatory mechanism of gene expression of each phase of the cell cycle may vary depending on the presence of CDK4, as the CDK4i condition showed altered kinetics in the entry and durations (Fig. 4A). Therefore, transcriptome and epigenetic analyses were conducted to investigate the molecular mechanisms responsible for cell cycle regulation post-CDK4 inhibition. To elucidate the changes in gene expression patterns induced by the inhibitor, we analyzed time-course mRNA expression (control, 2, 4, 8, 12, 16, 20, 24, and 28 h after HRG stimulation) as well as H3K27Ac and H3K4me1 modification (control, 16, 20, 24, and 28 h after HRG stimulation) in the presence or absence of CDK4i. First, active transcription factors were predicted based on the RNA-seq data at each time point using DoRothEA (*48*) (Fig. S4A). mRNAs corresponding to transcription factors, such as *Myc*, AP-1 family (*Jun*, *Fos*), *EGR1*, *NFKB1*, and *STAT3*, which are known to promote cell cycle progression (*26*, *28*, *30*, *49*, *50*) were highly enriched 4 h after CDK4i treatment (16 h after HRG stimulation).

Next, motif enrichment analysis was performed to confirm whether these transcription factors bind to promoter regions. Here, we defined the regions where the H3K27Ac peak signal did not overlap with the H3K4me1 peak signal as the active promoter region (*51*, *52*) (Fig. S4B and C). The analysis revealed that E-box sequences (CANNTG) (*53*) were enriched in the promoter regions at all time points following CDK4i treatment (Fig. 4B). Given that c-Myc is known to bind E-box sequences (*54*), we focused on its role in G1/S transition during CDK4 inhibition.

Near the R point (12–16 h after HRG stimulation) in CDK4i-non-treated cells, both c-Myc

protein and p-c-Myc (Ser^{62}) levels decreased (Fig 2A and B). Additionally, gene set enrichment analysis (GSEA), using normalized enrichment scores (NESs) (*55*), did not show any significant enrichment of Myc-target genes during 12-16 h in the same condition (Fig. 4C). However, 4 h after treatment with CDK4i (16 h after HRG stimulation), Myc-target genes were significantly enriched compared to the untreated cells (Fig. 4D). However, no significant difference was observed between the CDK4i and control conditions at later time points (24–28 h). Since c-Myc-target genes include a broad range of genes beyond those related to the cell cycle, detecting significant differences is challenging. Therefore, we focused on examining the temporal expression patterns of individual cell cycle-related genes within the c-Myc-target genes.

Specifically, we focused on genes whose promoter region exhibited a higher abundance of H3K27Ac modification than their enhancer region (Fig. S4D). The results showed that *CCNE1* expression was significantly enhanced 16 h after HRG stimulation in the presence of CDK4i, whereas the expression of *CCND1*, *CDK1*, *CDC25A*, *E2F2*, *E2F3*, and *CDKN1B* was not specific to the 16 h point and sustained over a longer period (20–28 h after HRG stimulation). These findings suggest that CDK4 inhibition alters the H3K27Ac levels in the promoter regions of c-Myc-target genes near the R point, leading to sustained expression of cell cycle-related genes. Therefore, when the G1/S transition, originally regulated by the cyclin D1 and CDK4 complex, is inhibited by CDK4i, it is maintained by an alternative pathway facilitated by the c-Myc activity, altering the cell cycle dynamics.

To further confirm whether the delayed G1/S entry following CDK4i treatment was due to the activation of c-Myc, we tested the effects of an inhibitor of c-Myc transcriptional activity (EN4). In both MCF-7 and T47D cells after 30 h, the combination of CDK4i and EN4 resulted in a dose-dependent increase in the proportion of cells in the G1 phase and a reduction in the number of cells in the S/G2/M phases (Fig. 4E to H), while no change was observed with EN4 alone (Fig. S4E to H). These results suggest that the transcriptional activity of c-Myc is responsible for the delayed G1/S entry and the escape from cell cycle arrest in response to CDK4 inhibition.

To further validate these findings using clinical data, microarray data from patients with luminal A subtype of breast cancer who received long-term (16 weeks, $n = 23$) or short-term (4 weeks, $n = 26$) CDK4/6i therapy were retrospectively analyzed (*56*). *PCNA*, a target gene for both c-Myc and E2F involved in DNA replication during G1/S transition, showed a 0.5 $\log_2$ fold change (FC) between the long-term and short-term treatment groups (Fig. 4I). In our mRNA expression data, *PCNA* expression increased after CDK4i treatment from 4 to 12 h (16 to 24 h after HRG stimulation) relative to the control (Fig. 4J). Taken together, these data suggest that CDK4 inhibition-induced epigenetic modifications activate c-Myc-target genes, ultimately contributing to cell cycle maintenance of cancer cells (Fig. 4K).

CDK4i induces ErbB2 degradation and delays G1/S transition

c-Myc is known to promote G1/S transition and cell proliferation (*30*, *41*). Therefore, if the

transcriptional activity of c-Myc is enhanced by CDK4i at 16 h, the time to G1/S transition is unlikely to be extended. However, on the contrary, as our results in CDK4i non-responders showed a prolonged G1/S transition time (Fig. 3D and E; Fig. 4A), we examined whether the level of c-Myc protein expression was decreased after CDK4i treatment (Fig. 5A and B). Results showed a slight reduction in the c-Myc protein expression level, although the difference was not statistically significant compared to that in untreated cells. Additionally, the levels of phosphorylated ErbB2, ERK, and AKT, which induce c-Myc mRNA expression and stabilize the c-Myc protein, decreased after CDK4 inhibition (Fig. 5A and B). These data suggest that the CDK4i-induced downregulation of the ErbB2 pathway itself may cause the extended G1/S transition time in wild-type (WT) MCF-7 cells.

To investigate the mechanism responsible for the CDK4i-induced downregulation of the ErbB2 pathway, we focused on the Hsp90-chaperone system, particularly with respect to the stability and maturation of nascent ErbB2. As WT MCF-7 cells naturally express low levels of ErbB2, we constructed and used MCF-7 cells with moderate overexpression of ErbB2 (Fig. S5A and B). After confirming the unaltered expression of ErbB2, PY100 (pan-tyrosine phosphorylation for estimation of p-ErbB2 level), and Hsp90 under CDK4i condition (Fig. S5C to G), we examined the co-localization patterns of these proteins using Mander's coefficient and Pearson's R value. Compared to control conditions, CDK4i treatment reduced co-localization of Hsp90 with ErbB2 or PY100 (Fig. 5C to F). No significant difference was observed in the total number of nuclei in any of the images (Fig. S5H and I). These results suggest that CDK4i inhibited the interaction between Hsp90 and ErbB2, leading to ErbB2 misfolding. In addition, ErbB2 protein expression was reduced 8 h after CDK4i treatment (20 h after HRG stimulation; Fig. 5G and H; Fig. S5J); however, the levels of ErbB2 mRNA did not change regardless of CDK4i treatment (Fig. S5K). Therefore, we investigated whether the downregulation of ErbB2 was caused by its protein degradation and tested the proteasome inhibitor MG132. Upon MG132 treatment, ErbB2 expression remained unchanged compared to the control condition (Fig. 5G and H; Fig. S5K). This indicates that CDK4i disrupts the interaction between Hsp90 and ErbB2, triggering ErbB2 degradation (Fig. S5L). To confirm this, we treated cells with the Hsp90 inhibitor geldanamycin (GA) at a concentration that suppressed ErbB2 expression by 40%, similar to the effect of CDK4i (Fig. S5M and N). As a result, cell cycle progression was nearly completely halted, and there was no substantial delay in the G1/S transition (Movie S1). Taken together, the timing of the G1/S transition is primarily governed by the activation and stability of the ErbB2 receptor. The loss of ErbB2 protein stability following CDK4i treatment may impair the regulation of c-Myc-mediated G1/S transition, even when c-Myc is activated through epigenetic modification. This dysregulation of c-Myc could contribute to the delayed G1/S transition observed in the CDK4i-unresponsive WT MCF-7 cells (Fig. 5I).

High ErbB2 induces cell cycle arrest through repression of cyclin D1 via c-Myc under CDK4 inhibition

If ErbB2 protein instability contributes to the delayed G1/S entry in the absence of CDK4i conditions, ErbB2 overexpression could counteract this effect. To test this hypothesis, we generated MCF-7 cells with varying levels of ErbB2 expression, from moderate to high (Fig. S5A and B), and analyzed their cell cycle phase distribution using live imaging (Fig. 5J).

After CDK4i treatment, in cells with high ErbB2 expression, the proportion of cells in the S/G2/M phase was significantly reduced (OE-Moderate: 14.9%, OE-High: 12.5%; Fig. 5F), indicating cell cycle arrest. First, to unveil the mechanism underlying the cell cycle arrest under CDK4i condition, we examined the expression of cyclin D1, a key regulator of cell cycle progression or arrest (*1*) (Fig. 5A and B). The results showed a significant reduction in cyclin D1 expression and p-RB levels in cells with high ErbB2 expression following CDK4i treatment. Therefore, we next investigated the cause of decreased cyclin D1 levels in ErbB2-overexpressing cells following CDK4i treatment. p27 protein reportedly promotes the assembly of the cyclin D1/CDK4 complex in the G1 phase (*40*), while its expression is inhibited by p-AKT and c-Myc (*41*). Our data revealed that p27 expression decreased after CDK4i treatment in ErbB2-overexpressing cells, whereas p-AKT and c-Myc expression tended to increase post-treatment. In contrast, p-ERK levels remained unchanged in different conditions. These findings suggest that, in ErbB2-overexpressing cells, the enhanced p-AKT-c-Myc axis antagonizes the expression of p27 and cyclin D1, leading to cell cycle arrest, in the absence of CDK4 activity.

Reversible cell cycle arrest is sustained by c-Myc transcriptional activity

Drug resistance is closely linked to reversible cell cycle arrest (*11*). To investigate whether the cell cycle arrest induced by CDK4i treatment in high ErbB2 expression cells was reversible, we examined the expression of proteins regulating the G1/S transition and the percentage of cells progressing through the G1/S transition after CDK4i washout. The results showed that the cyclin D1, p27, and p-RB levels increased after CDK4i washout compared to those in no-washout cells; however, c-Myc expression remained unchanged (Fig. 6A and B).

Thus, c-Myc phosphorylation (Ser^{62}) was further validated at the single-cell level to confirm the elevated transcriptional activity of c-Myc in cell cycle–arrested cells. We also quantified the ratio of phosphorylated c-Myc (Ser^{62}) to cyclin D1 (p-c-Myc/cyclin D1) at the single-cell level, along with the percentage of cells in the S/G2/M phase based on changes in DAPI staining (Fig. 6C). Histograms showed that the p-c-Myc/cyclin D1 ratio was lower following CDK4i washout than following no-washout. Notably, the percentage of cells in the S phase increased from 18.7% to 47.5% following the CDK4i washout. The p-c-Myc/cyclin D1 ratio was also maintained in ErbB2-overexpressing cells compared to that in the WT (Fig. S6A). These findings imply that sustained cell cycle arrest in ErbB2-overexpressing cells may be due to the persistent transcriptional activation of c-Myc.

Furthermore, we investigated whether blocking c-Myc transcriptional activity could prevent reversible cell cycle arrest. After treating cells with or without EN4 under CDK4i conditions for

8 h and subsequent washing, we examined the ratio of cells in the G1 phase to those in the S/G2/M phase at 52 h (72 h after HRG stimulation; Fig. 6D and E). Notably, the combination of EN4 and CDK4i reduced the percentage of cells in the S/G2/M phase while increasing the percentage of cells in the G1 phase, suggesting an impairment of cell cycle re-entry. Further, although the p27 (*CDKN1B*) mRNA levels were reduced by CDK4i treatment, combining EN4 and CDK4i could rescue the p27 mRNA levels (Fig. 6F and G). This result also suggests that p27 mRNA levels were directly reduced by c-Myc transcriptional activity following CDK4i treatment. Overall, these data support the hypothesis that in cells expressing high levels of ErbB2, CDK4 inhibition leads to reversible cell cycle arrest due to an excessive increase in c-Myc transcriptional activity and a rapid decrease in cyclin D1, attributed to the reduction of p27.

Stable cell cycle arrest is also associated with the cellular senescence (*58*, *59*). ErbB2 is also known to induce senescence associated with p21 expression (*60*). Lastly, we examined the senescence phenotype of the cells under our experimental conditions. We assessed the extent of cellular senescence after 6 days of CDK4 inhibitor treatment, with or without EN4, by measuring the SA-β-Gal staining levels (Fig. 6 H and I). CDK4i induced SA-β-Gal activity in all the cell lines assessed; however, the staining levels decreased as ErbB2 expression levels increased. Furthermore, EN4 at 4 μM significantly increased SA-β-Gal staining in WT MCF-7 cells, showing greater effectiveness than CDK4 inhibitor treatment alone (Fig. 6 H and I). However, EN4 at 4 μM did not induce any additional changes in T47D cells or MCF-7 cells with high ErbB2-overexpression. This reflects the situation where, in WT MCF-7 cells, a low concentration of EN4 (2 nM) was sufficient to induce cell cycle arrest, but a notably higher concentration (2 μM) was needed to achieve the same effect in WT T47D cells (Fig. 4 E and F). Our results suggest that ErbB2 expression levels modulate the irreversibility of the G1/S transition under CDK4i treatment, and the addition of c-Myc inhibitor further enhances the irreversible cell cycle arrest (Fig. 6J).

DISCUSSION

In this study, through an extensive time-course analysis of luminal A breast cancer cells with high and low ErbB2 expression, we aimed to clarify how the oncogenic ErbB2 signal modulates G1/S transition in breast cancer cells. Overall, our study could offer a comprehensive view of the process, from ErbB2 receptor activation to cell cycle entry. The findings demonstrate that ErbB2 receptor levels modulate the relative roles of cyclin D1 and c-Myc in the G1/S transition, ultimately providing two distinct pathways for cell cycle progression or arrest in the presense of CDK4i.

The luminal A subtype accounts for 30% of breast cancer cases. Although these patients typically receive standard hormone therapy, CDK4/6 inhibitors are also commonly used in cases of more advanced or metastatic tumors (*5*, *16*). However, there is a challenge of heterogeneous drug responses. Notably, the ErbB2-overexpressing subpopulation has been identified within luminal A breast cancer cells, which were initially characterized by low ErbB2 expression (*24*). Given that these subpopulations occur relatively infrequently, at around 7% (*61*), identifying differences in cell cycle regulation, focusing on ErbB2 expression, is critical for improving cancer treatment. Long-term CDK4i treatment, commonly used for luminal A breast cancer, activates alternative pathways such as PI3K/AKT/mTOR signaling, androgen receptor signaling, and Hippo signaling (*13*, *14*, *18–20*), along with transcriptional reprogramming via non-coding RNAs (*21*, *61*), gradually leading to the development of drug resistance. To mitigate this resistance, it is essential to inhibit potential pathways that may act at the very early step of the cell cycle entry. To this end, we investigated how differences in ErbB2 within cells of the same luminal A subtype can alter the core cell cycle regulatory network and sensitivity to CDK4 inhibitors (Fig. 7A and B).

In this study, we analyzed the temporal dynamics of the cell cycle regulators and live-cell imaging data and observed that the roles of cyclin D1 and c-Myc, key regulators of the G1/S transition, vary depending on the expression status of ErbB2 under CDK4i treatment. This variation ultimately affects the timing and irreversibility of G1/S transition. In MCF-7 cells, a representative luminal A breast cancer cell line known for the low ErbB2 expression, the G1/S transition is normally regulated by the cyclin D1/CDK4 complex via Hsp90 (Fig. 5C to E; Fig. S5, C to O). Although CDK inhibitors are known to sequester Hsp90 and CDK4/6 (*62*), our results suggest that the function of Hsp90 is complemented by CDK4 activity and contributes to stabilizing the ErbB2 protein. This finding of a positive feedback mechanism provides valuable insights into the signal-dependent complexity of cell cycle regulation. Thus, CDK4 inhibition generally induces cell cycle arrest in most cells; however, in a subpopulation of CDK4i non-responders, the G1/S transition still occurs, but with delays due to epigenetic modification and increased c-Myc transcriptional activity and ErbB2 degradation (Fig. 4; Fig. 7A). Paradoxically, the enhanced transcriptional activity of c-Myc triggered by CDK4 inhibition in the presence of the Hsp90 inhibitor led to reversible cell cycle arrest (Fig. 6A to G) by rapidly reducing cyclin

D1 levels through the suppression of p27 expression. The expression of p27, which recruits cyclin D1 to the nucleus during the G1 phase, is also repressed by AKT and c-Myc (*41*). Therefore, in high ErbB2-expressing MCF-7 cells, with high levels of AKT and c-Myc activity, CDK4 inhibition increases the levels of free cyclin D1, rendering it more susceptible to degradation (*63–65*). This results in a hypophosphorylated RB state in ErbB2-overexpressing MCF-7 cells than WT cells, leading to cell cycle arrest due to a decrease in free E2F bound to c-Myc (Fig. 7B).

Conversely, c-Myc is known to regulate the cell survival pathway (*41*, *66*). In ErbB2-overexpressing MCF-7 cells, cell cycle arrest was reversible after CDK4 inhibition (Fig. 6D and E), suggesting that the transcriptional activity of c-Myc in this context promotes sustained cell survival. These findings suggest that co-treatment with inhibitors targeting the transcriptional activity of c-Myc and CDK4 may be necessary to induce irreversible cell cycle arrest (Fig. 6H and I). On the other hand, at the same concentration as the Myc inhibitor that promoted cellular senescence in WT MCF-7 cells, the percentage of cellular senescence level in WT T47D cells and ErbB2-overexpressing cells did not change compared to that in the respective control conditions. For drug response assessments, identifying the threshold point at which c-Myc switches from supporting cell survival to inducing irreversible cell cycle arrest in relation to ErbB2 expression levels could inform more effective drug treatment strategies for breast cancer.

Overall, our results suggest that evaluating the c-Myc to cyclin D1 ratio could provide quantitative insights into the varying sensitivity to CDK4is, without relying solely on observable cell proliferation rates or single biomarker gene analysis.

MATERIALS AND METHODS

Reagents

PD0325901, the MEKi, was purchased from FUJIFILM Wako Pure Chemical Corp. (Osaka, Japan); CDK4i V was purchased from Calbiochem (CA, USA); AKTi VIII was purchased from Cayman Chemical (Ann Arbor, MI, USA); EN4 (Myci) was purchased from Selleck Chemicals (Houston, TX, USA); Geldanamycin was purchased from FUJIFILM Wako Pure Chemical Corp (Osaka, Japan); blasticidin was purchased from Kaken Pharmaceutical (Tokyo, Japan); Lipofectamine LTX was purchased from Thermo Fisher Scientific (Thermo Fisher Scientific); HRG was procured from R&D Systems, Inc (MN, USA).

ErbB2 overexpression

The method for constructing MCF-7 (ATCC, HTB-22) overexpressing full-length human ErbB2 (HER2) is described as follows. A human ErbB2 cDNA in the pCMV6-XL5 vector was purchased from OriGene (Catalog No: TC128161, Rockville, MD). The cDNA fragment was cloned into the vector pCMV-6-Neo vector (OriGene). The plasmid was then transfected into MCF-7 cells using the Lipofectamine LTX (Invitrogen, Carlsbad, CA) according to the manufacturer's protocol, and stable transfectants were selected with G418 (neomycin). Colonies derived from single cells compartmentalized in 96-well plates were isolated and examined. The ErbB2 expression level was examined to obtain cells with moderate or high ErbB2 expression via western blotting as described below (protein extraction and immunoblotting).

Cell culture

MCF-7 and ErbB2-overexpressing MCF-7 cells were cultured in Dulbecco's modified Eagle's medium (DMEM, Nakalai Tesque, Kyoto, Japan) supplemented with 10% (v/v) fetal bovine serum (FBS, Sigma-Aldrich) and 1% penicillin-streptomycin (100 IU/mL penicillin, 100 μg/mL streptomycin; Nacalai Tesque, Kyoto, Japan) at 37 °C in a humidified 5% CO_2 atmosphere. MCF-7 and ErbB2-overexpressing MCF-7 cells were routinely tested using the CycleavePCR Mycoplasma Detection Kit (Takara bio, CY-232). None of the cell lines were contaminated with mycoplasma.

FUCCI transfection

MCF-7 cells and ERBB2-overexpressed MCF-7 cells stably expressing the FUCCI biosensor were generated using the PiggyBac transposase system (*67*). Lipofectamine LTX (Thermo Fisher Scientific, USA) was used to transfect FUCCI plasmid (pPBbsr2-H2B-iRFP-P2A-mScarlet-I-hGem-P2A-PIP-tag-NLS-mNeonGreen; https://benchling.com/s/seq-LPZ1tLdpgnpJIYOG2ujR) along with hyPBase (https://benchling.com/s/seq-oGkw53b41IZqvzF5yQ9K) into MCF-7 and ErbB2-overexpressing MCF-7 cells, as per following manufacturer's protocol (*68*). For separating cells that stably expressed the plasmid, cells were suspended in a drug-free medium for 48 h, followed by blasticidin treatment (10 μg/mL). Colonies derived from single cells compartmentalized in 96-well plates were selected by microscopic live-cell observation, which

showed Geminin and PIP-tag fluorescence.

Protein extraction and immunoblotting

Total cell lysates were prepared in RIPA buffer (Nakalai Tesque, 1648834) containing protease inhibitors (Roche, 11836153001) and phosphatase inhibitors (Roche, 4906837001) at 4 °C. Cells were vortexed for 5 min and centrifuged at 16,000 × g for 15 min at 4 °C, and the supernatant was collected. The supernatant was denatured by heating at 95 °C with sample buffer (5×) and 2-mercaptoethanol (Nakalai Tesque, 21418-55) for 5 min. SDS polyacrylamide gel electrophoresis (Nacalai Tesque, 1306644) was performed, and the proteins were transferred to polyvinylidene fluoride membranes (Merck, Germany) and incubated with 10% blocking buffer (Nacalai Tesque, 03953-95) prepared in Tris-buffered saline/Tween 20 (Takara Bio, T9142; TBS-T) for 1 h at 25 °C. Membranes were probed overnight with antibodies against AKT (1:1000; Cell Signaling Technology; #4685), p-AKT (Thr^{308}; 1:1000; Cell Signaling Technology; #2965), ERK (1:1000; Cell Signaling Technology; #9102), p-ERK (Thr^{202} Tyr^{204}; 1:1000; Cell Signaling Technology; #4370), HER2/ErbB2 (1:1000; Cell Signaling Technology; #2165), p-HER2/ErbB2 ($Thr^{1221/1222}$; 1:1000; Cell Signaling Technology; #2249), p-c-Fos (Ser^{374}; 1:1000; Abcam; #ab55836), c-Fos (1:200; Santa Cruz; #sc-166940), p-c-Myc (Ser^{62}; 1:1000; Abcam; #ab51156), c-Myc (1:200; Santa Cruz; #sc-40), E2F-1 (1:1000; Cell Signaling Technology; #3742), p-RB ($Ser^{807/811}$; 1:1000; Cell Signaling Technology; #8516), p-RB (Thr^{373}; 1:1000; Abcam; #ab52975), RB1 (1:1000; NOVUS biologicals; #SPM353), cyclin D1 (1:1000; Cell Signaling Technology; #2978), cyclin E (1:200; Santa Cruz; #sc-247), cyclin A (1:200; Santa Cruz; #sc-271682), CDK4 (1:1000; Santa Cruz; #DSC-35), CDK2 (1:1000; Santa Cruz; #D-12), P27 Kip1 (1:1000; Cell Signaling Technology; #3686), and GAPDH (1:4000; Proteintech, MA, USA; 10494-1-AP) in TBS-T including 10% blocking buffer at 4 °C. They were then incubated with horseradish peroxidase (HRP)-conjugated secondary antibodies: HRP-conjugated anti-mouse IgG (1:5000; Cell Signaling Technology; #7076) and HRP-conjugated anti-rabbit IgG (1:5000; Cell Signaling Technology; #7074) for 1 h at room temperature. The membranes were developed using a chemiluminescent HRP substrate (Merck, Germany). Protein bands were detected using an Amersham Imager 600 UV (GE Healthcare, Eindhoven, Netherlands) and visualized using ImageJ-Fiji software (version 2.14.0/1.54f, NIH).

qRT-PCR

qRT-PCR was conducted as described previously (*69*). RNA was isolated from cells using NucleoSpin RNA Plus (Macherey-Nagel, Duren, Germany, Cat. No. 740984.250) according to the manufacturer's protocol. cDNA was synthesized using the ReverTra Ace qPCR RT Master Mix (TOYOBO, Osaka, Japan), and quantitative PCR was performed using a KOD SYBR qPCR kit (TOYOBO) on a CFX96 Real-Time PCR System (Bio-Rad Laboratories, Hercules, CA, USA). The ΔΔCq method was used to quantify gene expression, using RPL27 expression as an internal reference (*70*). The primers used for real-time PCR are listed in Table S1.

Cell cycle analysis using the FUCCI biosensor

Cell cycle analysis was conducted as described previously (*69*). Time-lapse microscopy images were acquired using an IN Cell Analyzer 2500HS (GE Healthcare Life Science) equipped with a CFI S Plan Fluor ELWD dry objective lens 20× (NA: 0.45) using an excitation wavelength of 475 nm and an emission wavelength of 511 nm for PIP-tag-mNeonGreen, and an excitation wavelength of 542 nm and an emission wavelength of 597 nm for mScarlet-hGem. Cells were maintained at 37 °C in a humidified 5% CO_2 atmosphere and imaged at 20-min intervals for 72 h. Image processing and quantification of the percentage of cells in each cell cycle phase were performed using ImageJ-Fiji software (version 2.14.0/1.54f, NIH). Masks of the mScarlet-hGem and PIP-tag-mNeonGreen signals were obtained by applying a fixed threshold. The obtained masks were identified using 'Analyze Particles' and automatically counted as ROIs. Cell cycle phases were determined in the following manner: G1 phase, PIP-tag-positive; S phase, hGem-positive; G2/M phase, PIP-tag- and hGem-positive. The average brightness of mScarlet and mNeonGreen was obtained using cell-tracking software (Olympus). The threshold parameters for mScarlet and mNeonGreen for each cell were set manually. Subsequently, an algorithm for estimating the cell cycle phase assembled using R packages [brunnermunzel (v.1.4.1), multimode (v.1.4), rlist (v.0.4.6.1), and tidyverse (v.1.3.0)] was employed to determine the cell cycle phase at the single-cell level. The duration of each cell cycle phase was obtained from the single-cell data.

Nuclei count

The number of nuclei was quantified based on the fluorescence of the FUCCI probes, and a nuclear marker (histone H2B), mScarlet-hGem, and PIP-tag-mNeonGreen signals were used as an indicator of cell proliferation. Image processing and quantification of the nuclear ratio were performed using ImageJ-Fiji software (version 2.14.0/1.54f, NIH). Masks of the merged nuclear marker, mScarlet-hGem, and PIP-tag-mNeonGreen signals were obtained by applying a fixed threshold. The obtained masks were identified using 'Analyze Particles' and automatically counted as regions of interest (ROIs). The nuclear ratio was calculated by dividing the number of nuclei at the end of the imaging by the number of nuclei at the beginning. Thus, the nuclear ratio indicated potential cell cycle arrest if it was close to 1.0, cell proliferation if it exceeded 1.0, and apoptosis if it was less than 1.0.

Immunostaining and quantitative analysis of images

MCF-7 cells and cells overexpressing ErbB2 (moderate or high) were seeded in 12-well plates at a density of 200,000 cells per well and cultured in 10% FBS containing DMEM for 48 h. The medium was then changed to FBS-free phenol red-free DMEM (FUJIFILM Wako Pure Chemical Corp.), and the cells were cultured for 17 h. Then, the medium was changed again, and the cells were cultured for 3 h. After administration of 10 nM HRG (R&D Systems, Inc.) for 12 h, the cells were independently treated with CDK4i and dimethyl sulfoxide (DMSO). Cells were

washed twice with PBS at the indicated times and fixed for 2 min with pre-prepared methanol at -20 °C. They were washed twice with Blocking One (Nacalai Tesque, 03953-95) and incubated overnight at 4 °C with Blocking One. Next day, cells were incubated overnight at 4 °C with the primary antibodies diluted in 10% goat serum (Thermo Fisher Scientific, 16210064)/Blocking One. Following this, cells were washed five times with PBS and incubated with fluorescent dye–conjugated secondary antibody, 2 $\mu g \cdot mL^{-1}$ DAPI (Nacalai Tesque, 11034-56), and 0.5 $\mu g \cdot mL^{-1}$ CellMask™ (Thermo Fisher Scientific, H32721) for 1 h at room temperature. Cells were washed five times with PBS, and images were acquired using an IN Cell Analyzer 2500HS (GE Healthcare Life Science, USA) at 20× magnification. At least three images from each experimental condition, containing at least 100 cells, were used for quantification. Image quantification processing was performed using ImageJ-Fiji software (version 2.14.0/1.54f, NIH) and CellProfiler (ver. 4.2.1). Co-localization analysis for Hsp90 with either ErbB2 or pY100 was performed using the "Coloc 2" plugin in ImageJ-Fiji software. Cell fractionation was performed on CellMask™ stained images using CellProfiler, and the mean intensity values of p-c-Myc, cyclin D1 and DAPI in each cell were obtained. The ratio of phosphorylated c-Myc (Ser62) to cyclin D1 (p-c-Myc/cyclin D1) for each cell was plotted on the y-axis, and the DAPI intensity was plotted on the x-axis. The DAPI intensity indicating the G1/S transition was determined based on the percentage of cells that had be in the S/G2 /M phase 24 hours after HRG stimulation. In WT MCF-7, 22.4% of the cells were in the S/G2/M phase, and the DAPI intensity indicating G1/S transition at this time was 0.105. MCF-7 cells overexpressing ErbB2 (high levels) had 25.4% of their cells in the S/G2/M phase, and the DAPI intensity indicating the G1/S transition at this time was 0.0775.

Analysis of senescence associated β-galactosidase (SA-β-gal)-positive cells

SA-β-gal staining was conducted as described previously (*69*). Briefly, the senescent cells were stained by a senescence β-galactosidase staining Kit (#9860; Cell Signaling Technology), according to the manufacturer's instructions. Images were acquired with a Keyence BZ-9000 microscope (Keyence, Osaka, Japan) on 20× magnification. The percentage of SA-β-gal-positive cells was calculated from cell images using CellProfiler (ver. 4.2.1). The total number of cells was determined by visualizing nuclear segmentation with DAPI staining. The number of SA-β-gal-stained cells was identified using the UnmixColors module. The percentage of SA-β-gal-positive cells was then calculated as the ratio of SA-β-gal-stained cells to the total number of nuclei in each field of view.

RNA-seq

FUCCI-expressing MCF-7 cells were seeded in 6-well plates at a density of 450,000 cells per well and cultured in 10% FBS containing DMEM for 48 h. The medium was then changed to FBS-free phenol red-free DMEM, and the cells were cultured for 17 h. Then, the medium was changed again, and the cells were cultured for 3 h. After administration of 10 nM HRG for 12 h, the cells were independently treated with CDK4i and DMSO. Cells were washed twice with PBS

at the indicated times. Total RNA was isolated using NucleoSpin RNA Plus (Macherey-Nagel, Duren, Germany, Cat. No. 740984.250) at the respective specified time. Library construction and RNA-seq were performed on an Illumina sequencing platform (Rhelixa). Poly(A) RNA was prepared with the Poly(A) mRNA Magnetic Isolation Module (New England Biolabs, E7490), and the sequencing library was generated using the NEBNext® Ultra™II Directional RNA Library Prep Kit (New England Biolabs, E7760). RNA-seq was performed on NovaSeq 6000 (Illumina, USA) with 150-base pair (bp) paired-end reads. Raw reads were quality-checked using FastQC (version 0.11.9) and trimmed using TrimGalore (version 0.6.0) (*71*). Trimmed reads were mapped using STAR (version 2.7.9a) (*72*) with GRCh38 as the reference genome. featureCounts (version 1.6.4) (*73*) was used to construct the count matrix with parameters as "-p -B -t exon -g gene_name." Raw counts were converted to Transcripts Per Kilobase Million (TPM) and corrected using EdgeR (version 3.36.0) (*74*). Principal component analysis (PCA) was performed using the prcomp() function in R (version 4.1.1) (*75*). GSEA was performed using the fgsea package (version 1.20.0) (*76*) and the hallmark gene set in the Human MSigDB Collections (*55*).

ChIP-seq

FUCCI-expressing MCF-7 cells were seeded in 100 mm dishes at a density of 2,300,000 cells per dish and cultured in 10% FBS containing DMEM for 48 h. The medium was then changed to FBS-free phenol red-free DMEM, and the cells were cultured for 17 h. Next, the medium was changed, and the cells were cultured for 3 h. After administration of 10 nM HRG for 12 h, the cells were independently treated with CDK4i and DMSO. Cells were washed twice with PBS at the indicated times. Cells were fixed with 1% formaldehyde (Thermo Fisher Scientific) for 5 min. Fragmented DNA was obtained using a SimpleChIP(R) Plus Enzymatic Chromatin IP (CST, 9005) kit and an M220-focused ultrasonicator (Covaris). Immunoprecipitated DNA was obtained using the Auto iDeal ChIP-seq kit for Histones ×24 (Diagenode) on the SX-8G platform (Diagenode). Next, 2 µg anti-H3K27Ac antibody (Diagenode) and 2 µg anti-H3K4me1 antibody (Diagenode) were mixed with 10 µL DiaMag Protein A-coated magnetic beads, and IP reactions with DNA were performed for 12 h. De-crosslinking was conducted using 4 µl of 5 M NaCl and 1 µl of 20 mg/ml proteinase K (Thermo Fisher Scientific) for 4 h at 60 °C. Library construction and RNA-seq were performed using an Illumina sequencing platform (Rhelixa). A sequencing library was generated using the NEBNext Ultra II DNA Library Prep Kit for Illumina (New England Biolabs, 7645). ChIP-seq was performed on NovaSeq 6000 (Illumina, USA) with 150-base pair (bp) paired-end reads. H3K27Ac ChIP-seq and H3K4me1 data were processed using the same protocol as for RNA-seq. FastQC (version 0.11.9) was used for quality control. Trimming was performed using Trimmomatic (version 0.39) (*77*) with the following parameters: ILLUMINACLIP, TruSeq2-SE; fa, 2:30:10; LEADING, 30; TRAILING, 30; SLIDINGWINDOW, 4:15; MINLEN, 30; HEADCROP, 2. Reads were mapped using Bowtie2 (version 2.4.4) (*78*) with GRCh38 as the reference genome, and duplicate reads were excluded

using Picard (version 2.26.6) (*79*). Bigwig files were created from the generated BAM files using deepTools (version 3.5.1; bamCoverage function) (*80*). Peak regions were identified using HOMER (version 4.11) (*81*) with parameters "-style histone -L 0 -fdr 0.00005". All detected peak regions were annotated to their nearest neighbor genes using HOMER annotatePeaks.pl (version 4.11).

Promoter and enhancer detection

Promoter regions were defined as the regions in the H3K27Ac peak that did not overlap with the H3K4me1 peak and were within 250 bp of the transcription start site (TSS; at the center of the peak). Enhancer regions were defined as the regions in the H3K27Ac peak overlapping with the H3K4me1 peak and were more than 250 bp from the TSS, which was at the center of the peak. The TSS was obtained from the Ensembl database using BiomaRt (version 2.50.3) (*82*). The bed files containing the promoter and enhancer regions for all time points were merged, and the time-course of the coverage values of H3K27Ac ChIP-seq was calculated using HOMER annotatePeaks.pl (version 4.11). The estimated coverage values were used to detect promoters and enhancers affected by the CDK4i. Promoters that gained or lost signal due to CDK4i were defined as those with H3K27Ac ChIP-seq coverage values of $|\log_2 FC| > 0.3$ for inhibitor and control conditions. Enhancers that gained or lost signals due to CDK4i were defined as those that changed the coverage value of H3K27Ac ChIP-seq by $|\log_2 FC| > 0.3$ and target gene expression changes $|\log_2 FC| > 0.2$ in the same direction as the change in enhancer activity.

Motif analysis of ChIP-seq data

Motif analysis was performed using MEME Suite SEA (version 5.4.1) (*83*). The motif files were obtained from the JASPAR 2022 database (JASPAR2022_CORE_vertebrates_ nonredundant _v2) (*84*). Peak regions containing motifs were detected using the MEME Suite FIMO (version 5.4.1). The analysis was performed using default parameters.

Transcription factor enrichment analysis

Transcription factor analysis using the DoRothEA (version 1.6.0) (*48*) was conducted with the "run_viper" function from the DoRothEA package. Regulon data with a "confidence" level of A and B were used. Target genes were selected based on those that showed changes with an FDR < 0.01 between Control and Inhibition at each time point.

Clinical data analysis

Microarray gene expression data (GEO GSE93204) from biopsy samples from the NeoPalAna clinical trial (NCT01723774) (*56*) were used, and differentially expressed genes were analyzed using *P*-values adjusted using the Benjamini–Hochberg method that is employed to control the false discovery rate in GEO2R.

Statistical analysis

Statistical analysis and data visualization were performed in R (version 4.2.1) to assess normality

for the Kolmogorov–Smirnov test. If the data set followed a normal distribution, Student's t-test, and Welch's two-sample t-test were used after confirming equal variances using the F-test for comparisons between two groups. One-way analysis of variance (ANOVA) for more than two groups was followed by Tukey's post-hoc test. If the data set did not follow a normal distribution, a Kruskal–Wallis test or Mann–Whitney U test was used. P-values < 0.05 were considered significant.

Supplementary Materials

Fig. S1. Estimation of cell-cycle dynamics by tracking single cells.

Fig. S2. Expression dynamics of signaling molecules and cell cycle regulators.

Fig. S3. Effect of CDK4, AKT, and MEK inhibitors on the expression of cell-cycle regulators and cell-cycle phase distribution.

Fig. S4. Transcriptomic and epigenetic analysis to detect transcriptional regulation associated with CDK4 inhibition.

Fig. S5. The G1/S transition requires the stability of ErbB2 protein via Hsp90.

Fig. S6. A sustained p-c-Myc/cyclin D1 ratio was observed in ErbB2-overexpressing cells compared to control cells.

Table S1. The primers used for real-time PCR.

Movie S1. Hsp90 inhibitor geldanamycin (GA) halted cell cycle progression.

References and Notes:

1. A. Zetterberg, O. Larsson, Kinetic analysis of regulatory events in G1 leading to proliferation or quiescence of Swiss 3T3 cells. *Proc. Natl. Acad. Sci. U. S. A.* **82**, 5365–5369 (1985).

2. S. M. Rubin, J. Sage, J. M. Skotheim, Integrating Old and New Paradigms of G1/S Control. *Mol. Cell* **80**, 183–192 (2020).

3. H. K. Matthews, C. Bertoli, R. A. M. de Bruin, Cell cycle control in cancer. *Nat. Rev. Mol. Cell Biol.* **23**, 74–88 (2022).

4. Q. Yu, Y. Geng, P. Sicinski, Specific protection against breast cancers by cyclin D1 ablation. *Nature* **411**, 1017–1021 (2001).

5. T. Adon, D. Shanmugarajan, H. Y. Kumar, CDK4/6 inhibitors: a brief overview and prospective research directions. *RSC Adv.* **11**, 29227–29246 (2021).

6. U. Asghar, A. K. Witkiewicz, N. C. Turner, E. S. Knudsen, The history and future of targeting cyclin-dependent kinases in cancer therapy. *Nat. Rev. Drug Discov.* **14**, 130–146 (2015).

7. B. Weigelt, J. L. Peterse, L. J. van 't Veer, Breast cancer metastasis: markers and models. *Nat. Rev. Cancer* **5**, 591–602 (2005).

8. C. M. Perou, T. Sørlie, M. B. Eisen, M. van de Rijn, S. S. Jeffrey, C. A. Rees, J. R. Pollack, D. T. Ross, H. Johnsen, L. A. Akslen, O. Fluge, A. Pergamenschikov, C. Williams, S. X. Zhu, P. E. Lønning, A. L. Børresen-Dale, P. O. Brown, D. Botstein, Molecular portraits of human breast tumours. *Nature* **406**, 747–752 (2000).

9. T. Sørlie, C. M. Perou, R. Tibshirani, T. Aas, S. Geisler, H. Johnsen, T. Hastie, M. B. Eisen, M. van de Rijn, S. S. Jeffrey, T. Thorsen, H. Quist, J. C. Matese, P. O. Brown, D. Botstein, P. E. Lønning, A. L. Børresen-Dale, Gene expression patterns of breast carcinomas distinguish tumor subclasses with clinical implications. *Proc. Natl. Acad. Sci. U. S. A.* **98**, 10869–10874 (2001).

10. R. S. Finn, J. Dering, D. Conklin, O. Kalous, D. J. Cohen, A. J. Desai, C. Ginther, M. Atefi, I. Chen, C. Fowst, G. Los, D. J. Slamon, PD 0332991, a selective cyclin D kinase 4/6 inhibitor, preferentially inhibits proliferation of luminal estrogen receptor-positive human breast cancer cell lines in vitro. *Breast Cancer Res.* **11**, R77 (2009).

11. F. Lüönd, S. Tiede, G. Christofori, Breast cancer as an example of tumour heterogeneity and

tumour cell plasticity during malignant progression. *Br. J. Cancer* **125**, 164–175 (2021).

12. N. McGranahan, C. Swanton, Clonal Heterogeneity and Tumor Evolution: Past, Present, and the Future. *Cell* **168**, 613–628 (2017).

13. C. Michaloglou, C. Crafter, R. Siersbaek, O. Delpuech, J. O. Curwen, L. S. Carnevalli, A. D. Staniszewska, U. M. Polanska, A. Cheraghchi-Bashi, M. Lawson, I. Chernukhin, R. McEwen, J. S. Carroll, S. C. Cosulich, Combined Inhibition of mTOR and CDK4/6 Is Required for Optimal Blockade of E2F Function and Long-term Growth Inhibition in Estrogen Receptor–positive Breast Cancer. *Mol. Cancer Ther.* **17**, 908–920 (2018).

14. M. T. Herrera-Abreu, M. Palafox, U. Asghar, M. A. Rivas, R. J. Cutts, I. Garcia-Murillas, A. Pearson, M. Guzman, O. Rodriguez, J. Grueso, M. Bellet, J. Cortés, R. Elliott, S. Pancholi, C. J. Lord, J. Baselga, M. Dowsett, L.-A. Martin, N. C. Turner, V. Serra, Early Adaptation and Acquired Resistance to CDK4/6 Inhibition in Estrogen Receptor–Positive Breast Cancer. *Cancer Res.* **76**, 2301–2313 (2016).

15. S. Pancholi, R. Ribas, N. Simigdala, E. Schuster, J. Nikitorowicz-Buniak, A. Ressa, Q. Gao, M. F. Leal, A. Bhamra, A. Thornhill, L. Morisset, E. Montaudon, L. Sourd, M. Fitzpatrick, M. Altelaar, S. R. Johnston, E. Marangoni, M. Dowsett, L.-A. Martin, Tumour kinome re-wiring governs resistance to palbociclib in oestrogen receptor positive breast cancers, highlighting new therapeutic modalities. *Oncogene* **39**, 4781–4797 (2020).

16. A. Polk, I. L. Kolmos, I. Kümler, D. L. Nielsen, Specific CDK4/6 inhibition in breast cancer: a systematic review of current clinical evidence. *ESMO Open* **1**, e000093 (2016).

17. J. L. Dean, C. Thangavel, A. K. McClendon, C. A. Reed, E. S. Knudsen, Therapeutic CDK4/6 inhibition in breast cancer: key mechanisms of response and failure. *Oncogene* **29**, 4018–4032 (2010).

18. E. S. Knudsen, V. Kumarasamy, A. Ruiz, J. Sivinski, S. Chung, A. Grant, P. Vail, S. S. Chauhan, T. Jie, T. S. Riall, A. K. Witkiewicz, Cell cycle plasticity driven by MTOR signaling: integral resistance to CDK4/6 inhibition in patient-derived models of pancreatic cancer. *Oncogene* **38**, 3355–3370 (2019).

19. W. Ji, Y. Shi, X. Wang, W. He, L. Tang, S. Tian, H. Jiang, Y. Shu, X. Guan, Combined Androgen receptor blockade overcomes the resistance of breast cancer cells to palbociclib. *Int. J. Biol. Sci.* **15**, 522–532 (2019).

20. Z. Li, P. Razavi, Q. Li, W. Toy, B. Liu, C. Ping, W. Hsieh, F. Sanchez-Vega, D. N. Brown, A. F. Da Cruz Paula, L. Morris, P. Selenica, E. Eichenberger, R. Shen, N. Schultz, N. Rosen,

M. Scaltriti, E. Brogi, J. Baselga, J. S. Reis-Filho, S. Chandarlapaty, Loss of the FAT1 Tumor Suppressor Promotes Resistance to CDK4/6 Inhibitors via the Hippo Pathway. *Cancer Cell* **34**, 893-905.e8 (2018).

21. Z. Cai, Q. Shi, Y. Li, L. Jin, S. Li, L. L. Wong, J. Wang, X. Jiang, M. Zhu, J. Lin, Q. Wang, W. Yang, Y. Liu, J. Zhang, C. Gong, H. Yao, Y. Yao, Q. Liu, LncRNA EILA promotes CDK4/6 inhibitor resistance in breast cancer by stabilizing cyclin E1 protein. *Sci Adv* **9**, eadi3821 (2023).

22. J. S. Ross, J. A. Fletcher, The HER-2/neu Oncogene in Breast Cancer: Prognostic Factor, Predictive Factor, and Target for Therapy. *Oncologist* **3**, 237–252 (1998).

23. A. Lenferink, D. Busse, W. Flanagan, F. Yakes, C. Arteaga, ErbB2/neu kinase modulates cellular p27(Kip1) and cyclin D1 through multiple signaling pathways. *Cancer Res.* **61**, 6583–6591 (2001).

24. K. M. Turner, S. K. Yeo, T. M. Holm, E. Shaughnessy, J.-L. Guan, Heterogeneity within molecular subtypes of breast cancer. *Am. J. Physiol. Cell Physiol.* **321**, C343–C354 (2021).

25. M. M. Moasser, The oncogene HER2: its signaling and transforming functions and its role in human cancer pathogenesis. *Oncogene* **26**, 6469–6487 (2007).

26. Y. Yarden, M. X. Sliwkowski, Untangling the ErbB signalling network. *Nat. Rev. Mol. Cell Biol.* **2**, 127–137 (2001).

27. T. Nakakuki, M. R. Birtwistle, Y. Saeki, N. Yumoto, K. Ide, T. Nagashima, L. Brusch, B. A. Ogunnaike, M. Okada-Hatakeyama, B. N. Kholodenko, Ligand-specific c-Fos expression emerges from the spatiotemporal control of ErbB network dynamics. *Cell* **141**, 884–896 (2010).

28. P. M. Burch, Z. Yuan, A. Loonen, N. H. Heintz, An extracellular signal-regulated kinase 1- and 2-dependent program of chromatin trafficking of c-Fos and Fra-1 is required for cyclin D1 expression during cell cycle reentry. *Mol. Cell. Biol.* **24**, 4696–4709 (2004).

29. U. B. Keller, J. B. Old, F. C. Dorsey, J. A. Nilsson, L. Nilsson, K. H. MacLean, L. Chung, C. Yang, C. Spruck, K. Boyd, S. I. Reed, J. L. Cleveland, Myc targets Cks1 to provoke the suppression of p27Kip1, proliferation and lymphomagenesis. *EMBO J.* **26**, 2562-2574–2574 (2007).

30. P. Dong, M. V. Maddali, J. K. Srimani, F. Thélot, J. R. Nevins, B. Mathey-Prevot, L. You, Division of labour between Myc and G1 cyclins in cell cycle commitment and pace control. *Nat. Commun.* **5**, 1–11 (2014).

31. A. B. Pardee, A restriction point for control of normal animal cell proliferation. *Proc. Natl. Acad. Sci. U. S. A.* **71**, 1286–1290 (1974).

32. G. Yao, C. Tan, M. West, J. R. Nevins, L. You, Origin of bistability underlying mammalian cell cycle entry. *Mol. Syst. Biol.* **7**, 485 (2011).

33. S. L. Spencer, S. D. Cappell, F.-C. Tsai, K. W. Overton, C. L. Wang, T. Meyer, The proliferation-quiescence decision is controlled by a bifurcation in CDK2 activity at mitotic exit. *Cell* **155**, 369–383 (2013).

34. L. O. Murphy, J. P. MacKeigan, J. Blenis, A network of immediate early gene products propagates subtle differences in mitogen-activated protein kinase signal amplitude and duration. *Mol. Cell. Biol.* **24**, 144–153 (2004).

35. G. Leone, R. Sears, E. Huang, R. Rempel, F. Nuckolls, C.-H. Park, P. Giangrande, L. Wu, H. I. Saavedra, S. J. Field, M. A. Thompson, H. Yang, Y. Fujiwara, M. E. Greenberg, S. Orkin, C. Smith, J. R. Nevins, Myc Requires Distinct E2F Activities to Induce S Phase and Apoptosis. *Mol. Cell* **8**, 105–113 (2001).

36. J. A. Cornwell, A. Crncec, M. M. Afifi, K. Tang, R. Amin, S. D. Cappell, Loss of CDK4/6 activity in S/G2 phase leads to cell cycle reversal. *Nature* **619**, 363–370 (2023).

37. T. Lee, G. Yao, J. Nevins, L. You, Sensing and integration of Erk and PI3K signals by Myc. *PLoS Comput. Biol.* **4**, e1000013 (2008).

38. J.-C. Chambard, R. Lefloch, J. Pouysségur, P. Lenormand, ERK implication in cell cycle regulation. *Biochim. Biophys. Acta* **1773**, 1299–1310 (2007).

39. R. C. Muise-Helmericks, H. L. Grimes, A. Bellacosa, S. E. Malstrom, P. N. Tsichlis, N. Rosen, Cyclin D expression is controlled post-transcriptionally via a phosphatidylinositol 3-kinase/Akt-dependent pathway. *J. Biol. Chem.* **273**, 29864–29872 (1998).

40. M. D. Larrea, J. Liang, T. Da Silva, F. Hong, S. H. Shao, K. Han, D. Dumont, J. M. Slingerland, Phosphorylation of p27Kip1 regulates assembly and activation of cyclin D1-Cdk4. *Mol. Cell. Biol.* **28**, 6462–6472 (2008).

41. L. García-Gutiérrez, M. D. Delgado, J. León, MYC Oncogene Contributions to Release of Cell Cycle Brakes. *Genes* **10** (2019).

42. T. Nagashima, H. Shimodaira, K. Ide, T. Nakakuki, Y. Tani, K. Takahashi, N. Yumoto, M. Hatakeyama, Quantitative transcriptional control of ErbB receptor signaling undergoes graded to biphasic response for cell differentiation. *J. Biol. Chem.* **282**, 4045–4056 (2007).

43. H. Jeong, J. Kim, Y. Lee, J. H. Seo, S. R. Hong, A. Kim, Neuregulin-1 induces cancer stem cell characteristics in breast cancer cell lines. *Oncol. Rep.* **32**, 1218–1224 (2014).

44. G. D. Grant, K. M. Kedziora, J. C. Limas, J. G. Cook, J. E. Purvis, Accurate delineation of cell cycle phase transitions in living cells with PIP-FUCCI. *Cell Cycle* **17**, 2496–2516 (2018).

45. H. Imoto, M. Okada, Signal-dependent regulation of early-response genes and cell cycle: a quantitative view. *Current Opinion in Systems Biology* **15**, 100–108 (2019).

46. M. Chung, C. Liu, H. W. Yang, M. S. Köberlin, S. D. Cappell, T. Meyer, Transient Hysteresis in CDK4/6 Activity Underlies Passage of the Restriction Point in G1. *Mol. Cell* **76**, 562-573.e4 (2019).

47. S. Mueller, J. Huard, K. Waldow, X. Huang, L. A. D'Alessandro, S. Bohl, K. Börner, D. Grimm, S. Klamt, U. Klingmüller, M. Schilling, T160‐phosphorylated CDK2 defines threshold for HGF‐dependent proliferation in primary hepatocytes. *Mol. Syst. Biol.* **11**, 795 (2015).

48. L. Garcia-Alonso, C. H. Holland, M. M. Ibrahim, D. Turei, J. Saez-Rodriguez, Corrigendum: Benchmark and integration of resources for the estimation of human transcription factor activities. *Genome Res.* **31**, 745 (2021).

49. D. Joyce, C. Albanese, J. Steer, M. Fu, B. Bouzahzah, R. G. Pestell, NF-kappaB and cell-cycle regulation: the cyclin connection. *Cytokine Growth Factor Rev.* **12**, 73–90 (2001).

50. T. Hirano, K. Ishihara, M. Hibi, Roles of STAT3 in mediating the cell growth, differentiation and survival signals relayed through the IL-6 family of cytokine receptors. *Oncogene* **19**, 2548–2556 (2000).

51. J. Ernst, P. Kheradpour, T. S. Mikkelsen, N. Shoresh, L. D. Ward, C. B. Epstein, X. Zhang, L. Wang, R. Issner, M. Coyne, M. Ku, T. Durham, M. Kellis, B. E. Bernstein, Mapping and analysis of chromatin state dynamics in nine human cell types. *Nature* **473**, 43–49 (2011).

52. Roadmap Epigenomics Consortium, A. Kundaje, W. Meuleman, J. Ernst, M. Bilenky, A. Yen, A. Heravi-Moussavi, P. Kheradpour, Z. Zhang, J. Wang, M. J. Ziller, V. Amin, J. W. Whitaker, M. D. Schultz, L. D. Ward, A. Sarkar, G. Quon, R. S. Sandstrom, M. L. Eaton, Y.-C. Wu, A. R. Pfenning, X. Wang, M. Claussnitzer, Y. Liu, C. Coarfa, R. A. Harris, N. Shoresh, C. B. Epstein, E. Gjoneska, D. Leung, W. Xie, R. D. Hawkins, R. Lister, C. Hong, P. Gascard, A. J. Mungall, R. Moore, E. Chuah, A. Tam, T. K. Canfield, R. S. Hansen, R. Kaul, P. J. Sabo, M. S. Bansal, A. Carles, J. R. Dixon, K.-H. Farh, S. Feizi, R. Karlic, A.-R.

Kim, A. Kulkarni, D. Li, R. Lowdon, G. Elliott, T. R. Mercer, S. J. Neph, V. Onuchic, P. Polak, N. Rajagopal, P. Ray, R. C. Sallari, K. T. Siebenthall, N. A. Sinnott-Armstrong, M. Stevens, R. E. Thurman, J. Wu, B. Zhang, X. Zhou, A. E. Beaudet, L. A. Boyer, P. L. De Jager, P. J. Farnham, S. J. Fisher, D. Haussler, S. J. M. Jones, W. Li, M. A. Marra, M. T. McManus, S. Sunyaev, J. A. Thomson, T. D. Tlsty, L.-H. Tsai, W. Wang, R. A. Waterland, M. Q. Zhang, L. H. Chadwick, B. E. Bernstein, J. F. Costello, J. R. Ecker, M. Hirst, A. Meissner, A. Milosavljevic, B. Ren, J. A. Stamatoyannopoulos, T. Wang, M. Kellis, Integrative analysis of 111 reference human epigenomes. *Nature* **518**, 317–330 (2015).

53. Z. Liu, S. S. Venkatesh, C. C. Maley, Sequence space coverage, entropy of genomes and the potential to detect non-human DNA in human samples. *BMC Genomics* **9**, 509 (2008).

54. J. Guo, T. Li, J. Schipper, K. A. Nilson, F. K. Fordjour, J. J. Cooper, R. Gordân, D. H. Price, Sequence specificity incompletely defines the genome-wide occupancy of Myc. *Genome Biol.* **15**, 482 (2014).

55. A. Subramanian, P. Tamayo, V. K. Mootha, S. Mukherjee, B. L. Ebert, M. A. Gillette, A. Paulovich, S. L. Pomeroy, T. R. Golub, E. S. Lander, J. P. Mesirov, Gene set enrichment analysis: a knowledge-based approach for interpreting genome-wide expression profiles. *Proc. Natl. Acad. Sci. U. S. A.* **102**, 15545–15550 (2005).

56. C. X. Ma, F. Gao, J. Luo, D. W. Northfelt, M. Goetz, A. Forero, J. Hoog, M. Naughton, F. Ademuyiwa, R. Suresh, K. S. Anderson, J. Margenthaler, R. Aft, T. Hobday, T. Moynihan, W. Gillanders, A. Cyr, T. J. Eberlein, T. Hieken, H. Krontiras, Z. Guo, M. V. Lee, N. C. Spies, Z. L. Skidmore, O. L. Griffith, M. Griffith, S. Thomas, C. Bumb, K. Vij, C. H. Bartlett, M. Koehler, H. Al-Kateb, S. Sanati, M. J. Ellis, NeoPalAna: Neoadjuvant Palbociclib, a Cyclin-Dependent Kinase 4/6 Inhibitor, and Anastrozole for Clinical Stage 2 or 3 Estrogen Receptor–Positive Breast Cancer. *Clin. Cancer Res.* **23**, 4055–4065 (2017).

57. V. Gorgoulis, P. D. Adams, A. Alimonti, D. C. Bennett, O. Bischof, C. Bishop, J. Campisi, M. Collado, K. Evangelou, G. Ferbeyre, J. Gil, E. Hara, V. Krizhanovsky, D. Jurk, A. B. Maier, M. Narita, L. Niedernhofer, J. F. Passos, P. D. Robbins, C. A. Schmitt, J. Sedivy, K. Vougas, T. von Zglinicki, D. Zhou, M. Serrano, M. Demaria, Cellular senescence: Defining a path forward. *Cell* **179**, 813–827 (2019).

58. W. Huang, L. J. Hickson, A. Eirin, J. L. Kirkland, L. O. Lerman, Cellular senescence: the good, the bad and the unknown. *Nat. Rev. Nephrol.* **18**, 611–627 (2022).

59. T. M. Trost, E. U. Lausch, S. A. Fees, S. Schmitt, T. Enklaar, D. Reutzel, L. R. Brixel, P. Schmidtke, M. Maringer, I. B. Schiffer, C. K. Heimerdinger, J. G. Hengstler, G. Fritz, E. O. Bockamp, D. Prawitt, B. U. Zabel, C. Spangenberg, Premature senescence is a primary fail-

safe mechanism of ERBB2-driven tumorigenesis in breast carcinoma cells. *Cancer Res.* **65**, 840–849 (2005).

60. A. Prat, C. M. Perou, Deconstructing the molecular portraits of breast cancer. *Mol. Oncol.* **5**, 5–23 (2011).

61. W. Ji, W. Zhang, X. Wang, Y. Shi, F. Yang, H. Xie, W. Zhou, S. Wang, X. Guan, c-myc regulates the sensitivity of breast cancer cells to palbociclib via c-myc/miR-29b-3p/CDK6 axis. *Cell Death Dis.* **11**, 760 (2020).

62. S. T. Hallett, M. W. Pastok, R. M. L. Morgan, A. Wittner, K. L. I. M. Blundell, I. Felletar, S. R. Wedge, C. Prodromou, M. E. M. Noble, L. H. Pearl, J. A. Endicott, Differential regulation of G1 CDK complexes by the Hsp90-Cdc37 chaperone system. *Cell Rep.* **21**, 1386–1398 (2017).

63. J. P. Alao, The regulation of cyclin D1 degradation: roles in cancer development and the potential for therapeutic invention. *Mol. Cancer* **6**, 24 (2007).

64. K. Z. Guiley, J. W. Stevenson, K. Lou, K. J. Barkovich, V. Kumarasamy, T. U. Wijeratne, K. L. Bunch, S. Tripathi, E. S. Knudsen, A. K. Witkiewicz, K. M. Shokat, S. M. Rubin, p27 allosterically activates cyclin-dependent kinase 4 and antagonizes palbociclib inhibition. *Science* **366** (2019).

65. R. Sears, F. Nuckolls, E. Haura, Y. Taya, K. Tamai, J. R. Nevins, Multiple Ras-dependent phosphorylation pathways regulate Myc protein stability. *Genes Dev.* **14**, 2501–2514 (2000).

66. S. B. McMahon, MYC and the control of apoptosis. *Cold Spring Harb. Perspect. Med.* **4**, a014407 (2014).

67. K. Yusa, L. Zhou, M. A. Li, A. Bradley, N. L. Craig, A hyperactive piggyBac transposase for mammalian applications. *Proc. Natl. Acad. Sci. U. S. A.* **108**, 1531–1536 (2011).

68. S. Tabata, K. Matsuda, K. Nagai, Y. Izumi, M. Takahashi, Y. Motomura, A. I. Nagasato, S. Shimma, K. Moro, T. Bamba, M. Okada, Nuclear NFκB Activity Balances Purine Metabolism in Cellular Senescence, *bioRxiv* (2023)p. 2023.04.18.536673.

69. S. Tabata, K. Matsuda, S. Soeda, K. Nagai, Y. Izumi, M. Takahashi, Y. Motomura, A. Ichikawa Nagasato, K. Moro, T. Bamba, M. Okada, NFκB dynamics-dependent epigenetic changes modulate inflammatory gene expression and induce cellular senescence. *FEBS J.*, doi: 10.1111/febs.17227 (2024).

70. K. J. Livak, T. D. Schmittgen, Analysis of relative gene expression data using real-time quantitative PCR and the 2(-Delta Delta C(T)) Method. *Methods* **25**, 402–408 (2001).

71. M. Martin, Cutadapt removes adapter sequences from high-throughput sequencing reads. *EMBnet.journal* **17**, 10–12 (2011).

72. A. Dobin, C. A. Davis, F. Schlesinger, J. Drenkow, C. Zaleski, S. Jha, P. Batut, M. Chaisson, T. R. Gingeras, STAR: ultrafast universal RNA-seq aligner. *Bioinformatics* **29**, 15–21 (2013).

73. Y. Liao, G. K. Smyth, W. Shi, featureCounts: an efficient general purpose program for assigning sequence reads to genomic features. *Bioinformatics* **30**, 923–930 (2014).

74. M. D. Robinson, D. J. McCarthy, G. K. Smyth, edgeR: a Bioconductor package for differential expression analysis of digital gene expression data. *Bioinformatics* **26**, 139–140 (2010).

75. A Core Team (2021), *A Language and Environment for Statistical Computing. R Foundation for Statistical Computing, Vienna, Austria* (URL https://www.R-project.org/.).

76. G. Korotkevich, V. Sukhov, N. Budin, B. Shpak, M. N. Artyomov, A. Sergushichev, Fast gene set enrichment analysis, *bioRxiv* (2021)p. 060012.

77. A. M. Bolger, M. Lohse, B. Usadel, Trimmomatic: a flexible trimmer for Illumina sequence data. *Bioinformatics* **30**, 2114–2120 (2014).

78. B. Langmead, S. L. Salzberg, Fast gapped-read alignment with Bowtie 2. *Nat. Methods* **9**, 357–359 (2012).

79. *Picard* (http://broadinstitute.github.io/picard).

80. F. Ramírez, D. P. Ryan, B. Grüning, V. Bhardwaj, F. Kilpert, A. S. Richter, S. Heyne, F. Dündar, T. Manke, deepTools2: a next generation web server for deep-sequencing data analysis. *Nucleic Acids Res.* **44**, W160-5 (2016).

81. S. Heinz, C. Benner, N. Spann, E. Bertolino, Y. C. Lin, P. Laslo, J. X. Cheng, C. Murre, H. Singh, C. K. Glass, Simple combinations of lineage-determining transcription factors prime cis-regulatory elements required for macrophage and B cell identities. *Mol. Cell* **38**, 576–589 (2010).

82. S. Durinck, P. T. Spellman, E. Birney, W. Huber, Mapping identifiers for the integration of genomic datasets with the R/Bioconductor package biomaRt. *Nat. Protoc.* **4**, 1184–1191

(2009).

83. T. L. Bailey, J. Johnson, C. E. Grant, W. S. Noble, The MEME Suite. *Nucleic Acids Res.* **43**, W39-49 (2015).

84. J. A. Castro-Mondragon, R. Riudavets-Puig, I. Rauluseviciute, R. B. Lemma, L. Turchi, R. Blanc-Mathieu, J. Lucas, P. Boddie, A. Khan, N. Manosalva Pérez, O. Fornes, T. Y. Leung, A. Aguirre, F. Hammal, D. Schmelter, D. Baranasic, B. Ballester, A. Sandelin, B. Lenhard, K. Vandepoele, W. W. Wasserman, F. Parcy, A. Mathelier, JASPAR 2022: the 9th release of the open-access database of transcription factor binding profiles. *Nucleic Acids Res.* **50**, D165–D173 (2022).

Acknowledgments:

We thank all members of the Laboratory for Cell Systems at the Institute for Protein Research for discussions regarding this research and especially Mr. Kyoichi Ebata for helping to develop the cell cycle analysis. We also thank Mr. Hideya Aragaki from Olympus Corporation for providing the cell-tracking software.

Funding:

JSPS KAKENHI (18H04031, MO; 21K15503, ANI)

JST CREST Program (JPMJCR21N3, MO)

Uehara Memorial Foundation (MO)

Kaneko Narita Research Grant from the Protein Research Foundation (ANI)

New Field Development Support Program from the Institute for Protein Research (ANI)

Joint Research Grant from ExCELLS (MO, KA)

Author contributions:

Conceptualization: ANI, MO
Methodology: ANI, KM, KA, MO
Validation: ANI
Formal analysis: ANI, KM
Investigation: ANI, KM
Resources: ANI, KA, MO
Visualization: ANI, KM
Writing – Original Draft: ANI, KM, MO
Writing – Review & Editing: ANI, KM, KA, MO
Supervision: ANI, MO
Project administration: ANI, MO
Funding acquisition: ANI, KA, MO

Competing interests: The authors declare that they have no competing interests.

Data and materials availability: The sequence data for RNA-seq and ChIP-seq reported in this paper have been deposited in the DNA Data Bank of Japan with accession number ESUB001718. The code is available at https://github.com/okadalabipr/HER2_Cellcycle. All other data will be available upon reasonable request.

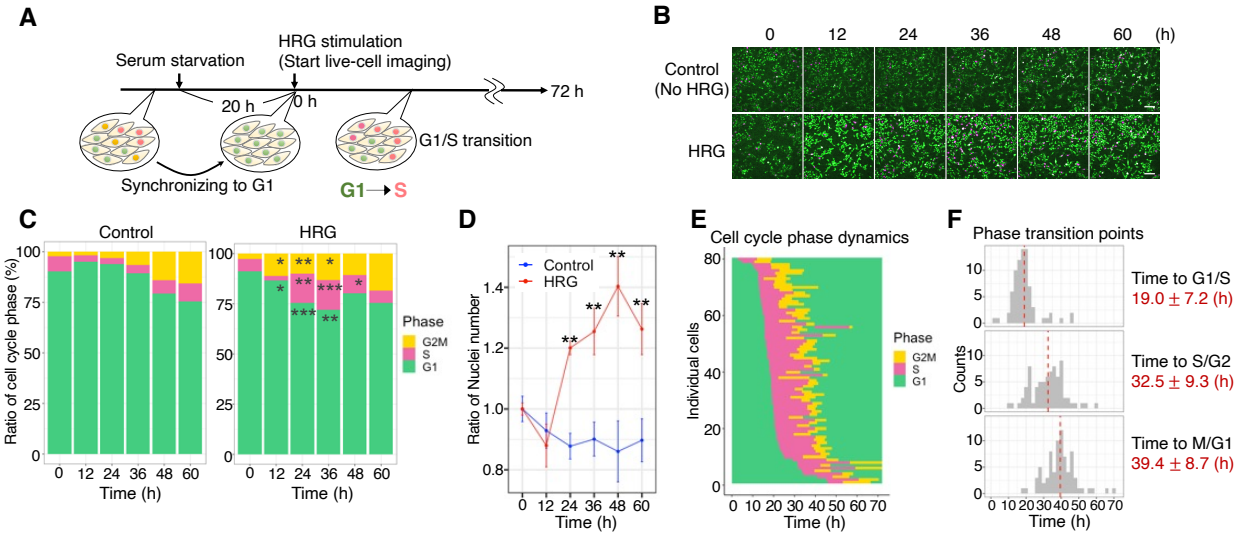

Fig. 1. G1/S transition occurs approximately 20 hours after HRG stimulation. (A – F) MCF-7 cells stably expressing FUCCI were used. (**A**) Experimental scheme for live-cell imaging using the FUCCI biosensor. (**B**) Images were captured every 20 min up to 72 h in conditions with or without 10 nM HRG. Scale bar: 100 µm. (**C**) Percentage distribution of each cell cycle phase (%) in each image; n = 3 for each image quantified. (**D**) The number of nuclei increased with each passing hour relative to the cell number at 0 h. (**E**) Cell cycle phase dynamics estimated based on Geminin and PIP fluorescence over time for each individual cell that could be followed up to 72 h; n = 79. (**F**) Histogram of each cell cycle transition time for n = 77 cells that completed the cell cycle within 72 h, based on the results in (E). Red dotted lines indicate the mean ± SE of each transition time. In (C) and (D), *P < 0.05, **P < 0.01, ***P < 0.001 (with respect to control and HRG; t-test).

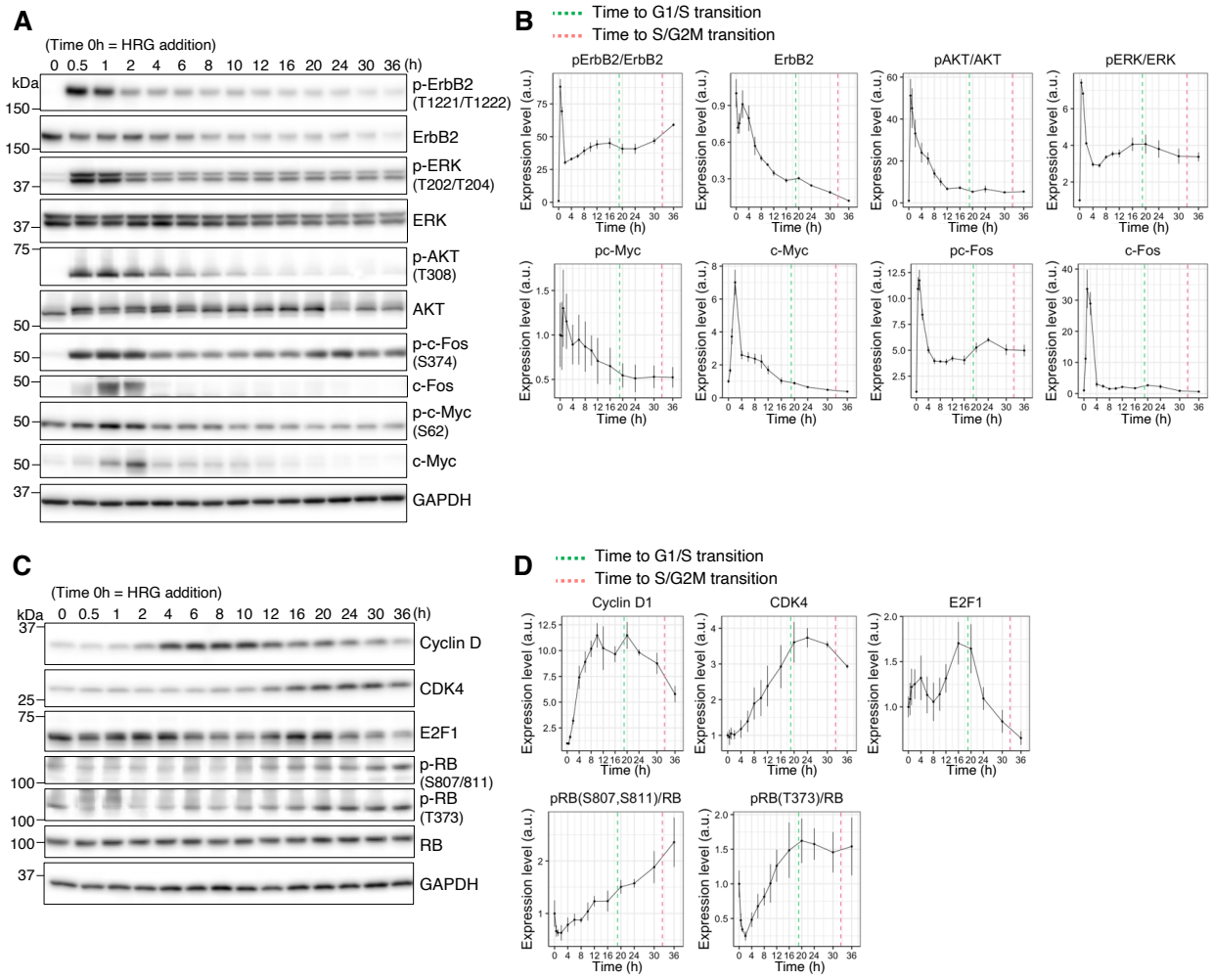

Fig. 2. Expression of CDK4 and cyclin D1 is expressed in a timely manner G1/S transition. (**A–D**) MCF-7 cells stably expressing FUCCI were used. Dynamics of changes in the expression or phosphorylation of individual proteins were detected by western blotting up to 36 h after treatment with 10 nM HRG; (**A, B**) ErbB2 signaling pathway proteins; (**C, D**) Proteins regulating the G1/S transition. The expression and phosphorylation levels of each protein were normalized relative to those of GAPDH; $n = 3$.

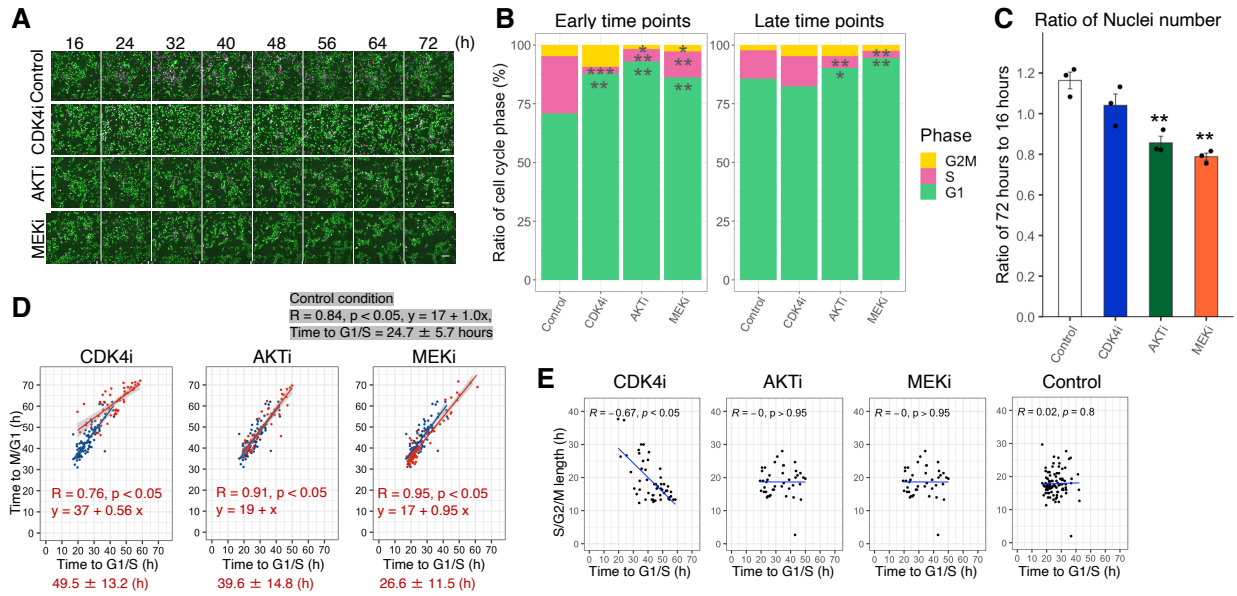

Fig. 3. A subset of the population enters the cell cycle even after CDK4 inhibition. (**A**) Each inhibitor (250 nM CDK4i; 600 nM AKTi; 500 nM MEKi) was used to treat the FUCCI stably expressing MCF-7 cells 12 h after HRG stimulation. Images were acquired every 20 min from 16 to 72 h after HRG stimulation. Scale bar: 100 µm. (**B**) Percentage distribution of each cell-cycle phase (%) in the overall image at early (32 h after HRG stimulation) and late (72 h after HRG stimulation) time points; $n = 3$. (**C**) The number of nuclei increased from 16 h to 72 h after HRG stimulation; $n = 3$. (**D**) Data from cells that completed the M/G1 transition within 72 h. Control; $n = 96$, CDK4i; $n = 52$, AKTi; $n = 42$, MEKi; $n = 75$. Time to G1/S and M/G1 transition is shown on the x-axis and y-axis, respectively, with slope (s) and intercept (i) obtained from the regression equation. (**E**) Comparison of Pearson coefficients using data from cells used in the analysis in (D), with the time to G1/S transition plotted on the x-axis and time to the S/G2/M phase plotted on the y-axis. In (B) to (C), $*P < 0.05$, $**P < 0.01$, $***P < 0.001$ (with respect to control and each inhibitor condition; *t*-test).

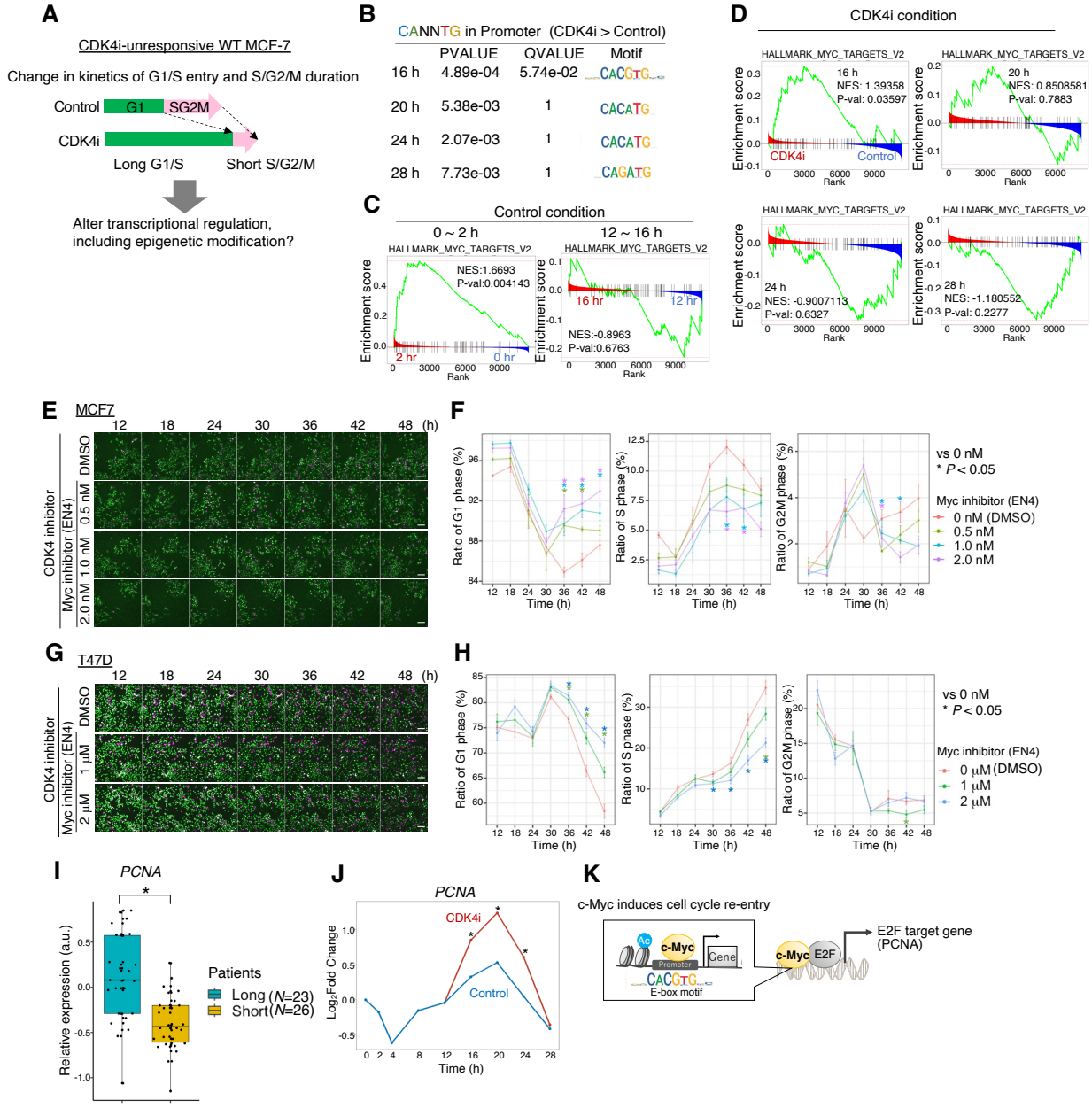

Fig. 4. CDK4i enhances c-Myc transcriptional activity via H3K27Ac modification. (**A**) Changes in cell-cycle distribution following CDK4 inhibition. (B-H, J) MCF-7 cells stably expressing FUCCI were used. (**B**) Motif-enrichment analysis of H3K27Ac modifications in the promoter region; E-box sequences (CANNTG) were enriched in the promoter region at all time points in the CDK4i-treatment group compared to controls. (**C**) GSEA was performed using the Myc-target gene set (n = 58) obtained from the Human MSigDB Collections. Comparison between 0–2 h after HRG stimulation (NES = 1.6693, P = 0.004143) and near the R point (12–16 h; NES = -0.8963, P = 0.6763). (**D**) GSEA was performed using the Myc-target gene set (C). Comparison between CDK4i and control conditions every 4 h of CDK4i treatment (16 h: NES = 1.39358, P = 0.03597; 20 h: NES = 0.8508581, P = 0.7883; 24 h: NES = -0.9007113, P = 0.6327; 28 h: NES = -1.180552, P = 0.2277). (**E–H**) After stimulation with 10 nM HRG for 11.5 hours, the cells were treated with 0

(DMSO)/0.5/1.0/2.0 nM EN4 (E, F) or 0 (DMSO)/1/2 μM EN4 (G, H) for 30 min. Subsequently, these MCF-7 cells (**E, F**) and T47D cells (**G, H**) were treated with 250 nM CDK4i. Scale bar: 100 μm. The percentage distribution of each cell cycle phase over time was quantified (**F, H**). (**I**) PCNA expression was analyzed using microarray data from luminal A subtype of breast cancer patients treated with CDK4/6i for the long term (16 weeks, $n = 23$) or short term (4 weeks, $n = 26$) (adj. P-value = 0.000132). (**J**) Expression of *PCNA* mRNA using RNA-seq data. (**K**) Increased c-Myc activity induces cell cycle re-entry to promote E2F target gene. In (F) and (H), $*P < 0.05$ (with respect to control and each inhibitor condition; t-test). In (I), $*P < 0.05$ [P-values calculated using the Benjamini–Hochberg method for controlling the false discovery rate in GEO2R]. In (J), $*P < 0.05$ (P-values were calculated using edgeR).

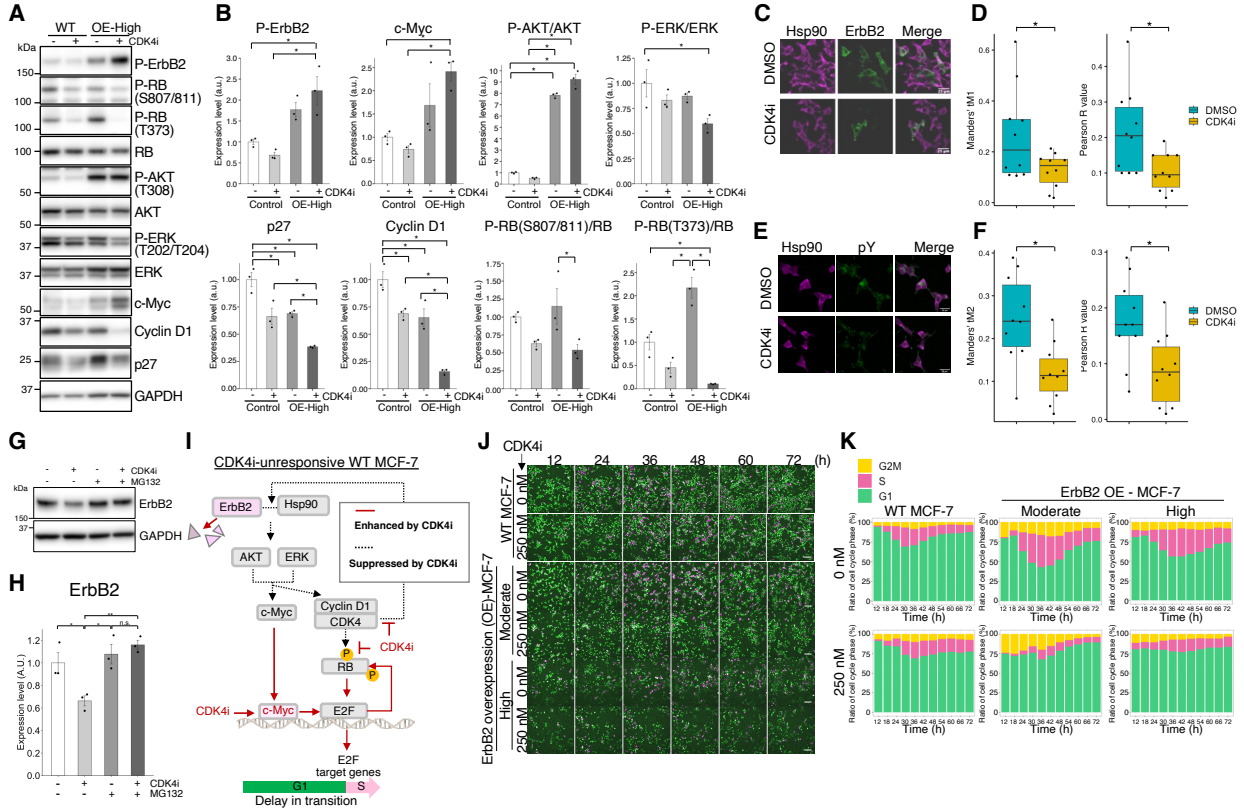

Fig. 5. High ErbB2 induces cell cycle arrest through repression of cyclin D1 via c-Myc under CDK4 inhibition. (**A, B**) WT MCF-7 and ErbB2-overexpressing MCF-7 cells (high levels) were treated with CDK4i or DMSO 12 h after HRG stimulation and then harvested at 24 h post-HRG stimulation. Western blotting results (A) showing p-ErbB2, p-RB (Ser$^{807/811}$), p-RB (Thr^{373}), RB, p-AKT (Thr^{308}), AKT, p-ERK (Thr^{202}/Thr^{204}), ERK, c-Myc, cyclin D1, and p27 expression (in control cells, i.e., DMSO treatment) after normalization with GAPDH (B). (**C**) Hsp90 and ErbB2 were co-stained by immunostaining. Scale bar: 25 µm. (**D**) Co-localization rate of Hsp90 and ErbB2 was evaluated by Mander's tM1 and Pearson's R value using coloc2 plugin of Image J; $n = 10$. (**E**) Hsp90 and pY100 were co-stained by immunostaining. Scale bar: 25 µm. (**F**) Co-localization rate of Hsp90 and pY100 was evaluated by Mander's tM2 and Pearson's R value using coloc2 plugin of Image J; $n = 10$. (**G, H**) Twelve hours after 10 nM HRG stimulation, FUCCI stably expressing MCF-7 cells were treated with CDK4i or DMSO (control), as well as 10 mM MG132 and collected 8 h later. (**G**) Expression of ErbB2 and GAPDH determined by western blotting. (**H**) ErbB2 normalized to GAPDH was quantified; $n = 3$. (**I**) In CDK4i-unresponsive WT MCF-7 cells, the loss of ErbB2 protein stability impair the regulation of c-Myc-mediated G1/S transition, leading to the delayed G1/S transition. (**J**) WT MCF-7 and ErbB2-overexpressing cells (moderate and high levels) were individually treated with 250 nM CDK4i or DMSO (no treatment) 12 h after stimulation with 10 nM HRG, and images were acquired every 20 min until 72 h after HRG stimulation. Scale bar: 100 µm. (**K**) Images in (J) were analyzed to quantitatively determine the proportion (%) of each cell cycle phase in the entire set of images; $n = 3$. In (B) and (H), $*P < 0.05$ (Tukey test). In (D) and (F), $*P < 0.05$ (with respect to control and CDK4i; t-test).

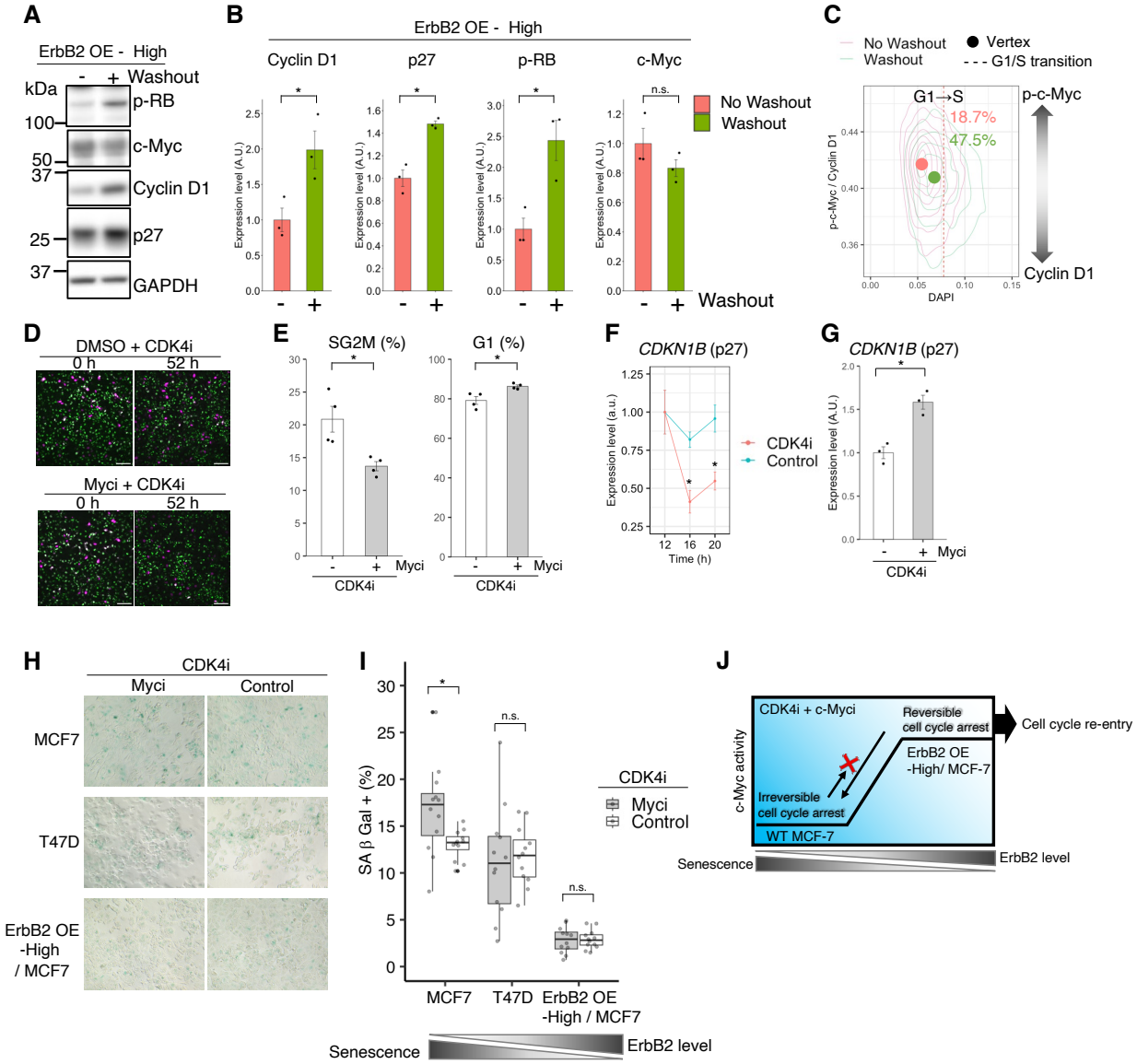

Fig. 6. Reversible cell cycle arrest is maintained under c-Myc transcriptional activity. (**A–G**) MCF-7 cells overexpressing ErbB2 (high levels) were used. (**A, B**) The following conditions were used: treatment with 250 nM CDK4i 12 h after HRG stimulation, followed by wash/no-wash treatment 4 h later; cells were harvested 40 h after HRG stimulation. Western blotting results showing the expression of p-RB, c-Myc, cyclin D1, p27, and GAPDH. After individually normalizing the proteins relative to GAPDH, the ratio to the no-wash condition was quantified; $n = 3$. (**C**) Washing operations were performed under the same conditions as in (A, B); cells were fixed 40 h after HRG stimulation and immunostained with p-c-Myc and cyclin D1 antibodies together with DAPI; $n = 3{,}859$. The x-axis shows the fluorescence intensity of DAPI, and the y-axis shows the p-c-Myc/cyclin D1 ratio. A higher value on the y-axis indicates that the amount of p-c-Myc in one cell was greater than that of cyclin D1. The circle shows the vertex of each histogram, and the red dotted line indicates the G1/S transition time point. (**D, E**) Cells were pre-treated for 30 minutes with/without 64 nM c-Myc inhibitor (EN4) 11.5 h after HRG stimulation. The cells were then incubated with 250 nM CDK4i for 8 h, washed, and

imaged 52 h later (72 h after HRG stimulation; D). (**E**) The percentage distributions of G1 and S/G2/M phases were examined based on the images in (D); $n = 3$. Scale bar: 100 µm. (**F**) Twelve hours after HRG stimulation, the cells were treated with 250 nM CDK4i or DMSO (control). mRNA levels of p27 up to 20 h after HRG stimulation were examined by qPCR; $n = 3$. (**G**) After the cells were treated with or without EN4 under the same conditions as in (D–E), RNA was collected 8 h after treatment with inhibitors, and the mRNA levels of *CDKN1B* were examined by qPCR; $n = 3$. (**H**) WT MCF-7, WT T47D and ErbB2 highly OE MCF-7 cells were pre-treated for 30 minutes with/without 4 mM c-Myc inhibitor (EN4) 11.5 h after HRG stimulation. The cells were then incubated with 250 nM CDK4i for 6 days and assessed SA b Gal staining level. (**I**) The percentage SA b Gal staining levels were examined based on the images in (H); $n = 12$. (**J**) ErbB2 expression levels modulate the irreversibility of the G1/S transition under CDK4i treatment. In (B), (E), (F), (G), (I) $^*P < 0.05$ (with respect to control and each inhibitor condition; *t*-test).

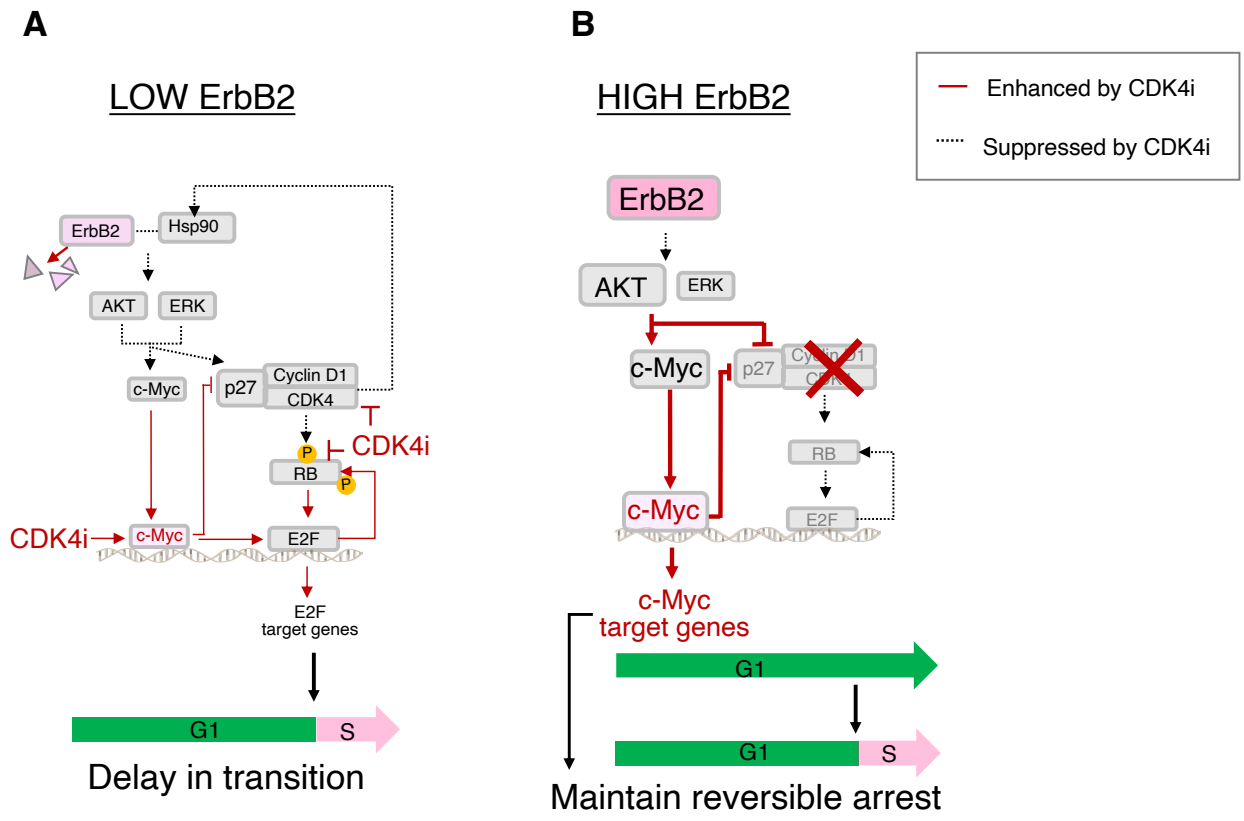

Fig. 7. Proposed model of the ErbB2 receptor regulation of G1/S transition via cyclin D1 and c-Myc in CDK4i non-responder cells. (**A**) In low ErbB2 cells, CDK4 inhibition leads to reduced pathway activity due to ErbB2 degradation via Hsp90 dis-colocalization. This event attenuated transcriptional activity of c-Myc activated by epigenetic changes. Consequently, a subpopulation of cells unresponsive to CDK4i exhibits a delayed G1/S transition. (**B**) In high ErbB2 cells, increased AKT activity leads to increased c-Myc expression. Subsequently, the expression of p27, which is critical for the stability of cyclin D1/CDK4 during the G1 phase, is suppressed by c-Myc, resulting in exhibiting a cell cycle arrest after CDK4 inhibition. This arrest is reversibly maintained by the strong transcriptional activity of c-Myc, ultimately sustaining survival signals.